Advances in Industrial and Manufacturing Engineering 6 (2023) 100121

Contents lists available at ScienceDirect

Advances in Industrial and Manufacturing Engineering

journal homepage: www.sciencedirect.com/journal/advances-in-industrial-and-manufacturing-engineering

Modelling of wire-arc additive manufacturing – A review

R.F.V. Sampaio [a], J.P.M. Pragana [a], I.M.F. Bragança [b], C.M.A. Silva [a], C.V. Nielsen [c], P.A.F. Martins [a,*]

[a] IDMEC, Instituto Superior Técnico, Universidade de Lisboa, Portugal
[b] CIMOSM, Instituto Superior de Engenharia de Lisboa, Instituto Politécnico de Lisboa, Portugal
[c] Department of Civil and Mechanical Engineering, Technical University of Denmark, Kgs, Lyngby, Denmark

ARTICLE INFO

Keywords:
Wire-arc additive manufacturing
Modelling
Macro-scale
Finite element method
State-of-the-art

ABSTRACT

This paper is focused on wire-arc additive manufacturing and has a twofold objective. First, to deliver an overall state-of-the-art review of the different aspects of modelling. Second, to provide a detailed analysis of the macro-scale finite element modelling. The methodology draws from the fundamentals of the macro, meso and micro-scale modelling of the process, to the main strategies and objectives behind the development of analytical, statistical, machine learning and finite element analyses of macro-scale modelling. The intention is to provide information on the pre-processing requirements, solution techniques and results that are currently being worked on by some of the leading researchers in the field. This will enable readers to understand the main challenges, relevance, and assumptions of the different published works. The theoretical and numerical aspects are intentionally kept in a clear and understandable level so that users of finite element computer programs having the know-how on wire-arc additive manufacturing can bridge the actual gap to the developers of the programs.

1. Introduction

Additive manufacturing processes can be subdivided into seven different categories according to the standard EN ISO/ASTM 52921 (2015). Four of these categories can be used to build metal parts through what is nowadays called metal additive manufacturing (MAM) (Fig. 1): powder bed fusion (PBF), direct energy deposition (DED), binder jetting (BJ) and sheet lamination (SL).

Powder bed fusion produces metal parts by slicing its geometry into layers and joining the individual particles of powder together, one layer at a time, according to a predefined path by means of a heat source obtained from a laser beam (PBF-LB) or an electron beam (PBF-EB) (Fig. 1a). The process has roots in selective laser sintering (SLS) that started to be developed in the late 1980's by Carl Deckard (1989) for the additive manufacturing of polymers.

Direct energy deposition produces metal parts by feeding powder or wire through a nozzle onto the build part where it is melted at the exact time of deposition by means of a heat source from a laser beam (DED-LB) (Fig. 1b), an electron beam (DED-EB), a plasma arc (DED-PA), a gas tungsten arc (DED-GTA), or a gas metal arc (DED-GMA). In contrast to PBF, the feedstock delivery system of powder or wire moves with the heat source along its predefined path, instead of remaining static inside the build platform during the construction of the part, layer-upon-layer. The roots of DED are found in the work of Dickens et al. (1992) to fabricate near net shape metal parts by combining electric arc welding machines with robots.

Binder jetting consists of spraying a stationary loose bed of powder placed on a build platform with a liquid adhesive through an inkjet style printer to stick the powders together into a cross-section, layer-upon-layer (Fig. 1c). The process was developed by Ely Sachs and co-workers (Sachs et al., 1993) and allows obtaining 'green parts' with low strength and approximately 60% relative density that are subsequently heated in a controlled atmosphere to remove the adhesive and sinter the individual particles of powder into a 'fully dense' metal part. Shrinking and loss of dimensional precision during sintering are the main drawbacks of binder jetting.

Sheet lamination joins thin metal sheets layer-upon-layer using ultrasonic welding or friction stir welding, to build an object that is subsequently cut according to the desired metal part geometry (Fig. 1d). The process has roots in laminated object manufacturing using paper as feedstock and melted plastic as adhesive bonding that was developed by Helisys Inc. in 1986.

* Corresponding author.
E-mail addresses: rui.f.sampaio@tecnico.ulisboa.pt (R.F.V. Sampaio), joao.pragana@tecnico.ulisboa.pt (J.P.M. Pragana), ibraganca@dem.isel.ipl.pt (I.M.F. Bragança), carlos.alves.silva@tecnico.ulisboa.pt (C.M.A. Silva), cvni@dtu.dk (C.V. Nielsen), pmartins@tecnico.ulisboa.pt (P.A.F. Martins).

https://doi.org/10.1016/j.aime.2023.100121
Received 27 February 2023; Received in revised form 3 May 2023; Accepted 7 May 2023
Available online 9 May 2023

In contrast to binder jetting (BJ) and sheet lamination (SL) that have a limited number of applications (DebRoy at el., 2018), both powder bed fusion (PBF) and direct energy deposition (DED) have a much broader usage. Fig. 2 provides guidelines on the utilization of PBF and DED, in which the former is preferred to make metal parts with higher resolution (Lee et al., 2017) but at slower build rates than DED (Vartanian et al., 2018) due to the larger melt pools created by the thermal heat sources of DED for the molten droplets to hit and solidify. This makes PBF suitable for making smaller parts with complex details and DED to scale more easily and cost-effectively to medium or larger size parts with less details, low dimensional accuracies, and high surface roughness.

The differences in part size applicability of wire and powder DED are due to the fact that wire-DED makes use of nearly 100% of the feedstock, whereas the capture efficiency of feedstock in powder-DED is below 90% (Ahn, 2021). This explains the higher deposition rates of wire-DED and justifies its use for the construction of larger metal parts (Fig. 2). The differences between powder and wire-DED gain additional meaning if the higher cost of materials supplied in the form of powder are considered (Dias et al., 2022).

On the other hand, the larger melt pools of wire-DED give rise to reduced end-part resolutions, limiting its applicability to simple geometries with few thin-to-thick transitions (Gibson et al., 2015).

Wire-arc additive manufacturing (WAAM) is a form of wire-DED (Fig. 3) that uses gas metal arc (GMA-DED) (Fig. 3a), gas tungsten arc (GTA-DED) (Fig. 3b) or plasma arc (PA-DED) (Fig. 3c), as heat sources and shares working principles with the well-established arc welding processes (Fig. 3). A major advantage of WAAM over other MAM

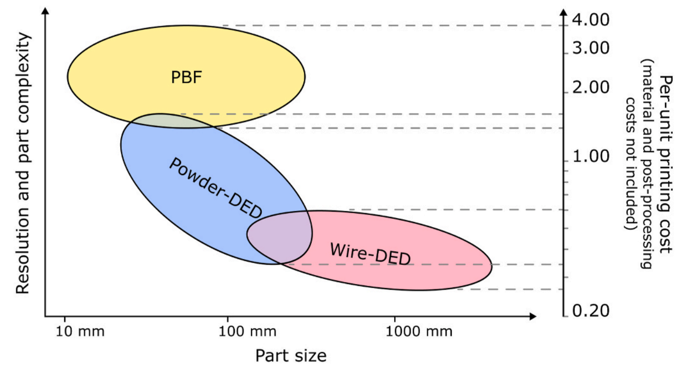

Fig. 2. Resolution, complexity, and per-unit printing costs (without material and post-processing costs) vs. part size for PBF and DED (adapted from Chu, 2014).

processes, which makes it very attractive in both industry and academia, is the lower capital investment and the ability to use equipment available from various suppliers of welding machines (Cunningham et al., 2018).

In fact, the combination of high material utilization, high deposition rates and low equipment cost of WAAM has been attracting the attention of industry to the creation of low to medium complexity and medium to large scale parts. Williams et al. (2016) provides several aerospace application examples covering wing spars, external landing gear assemblies and wing testing models, characterized by ratios of the mass of

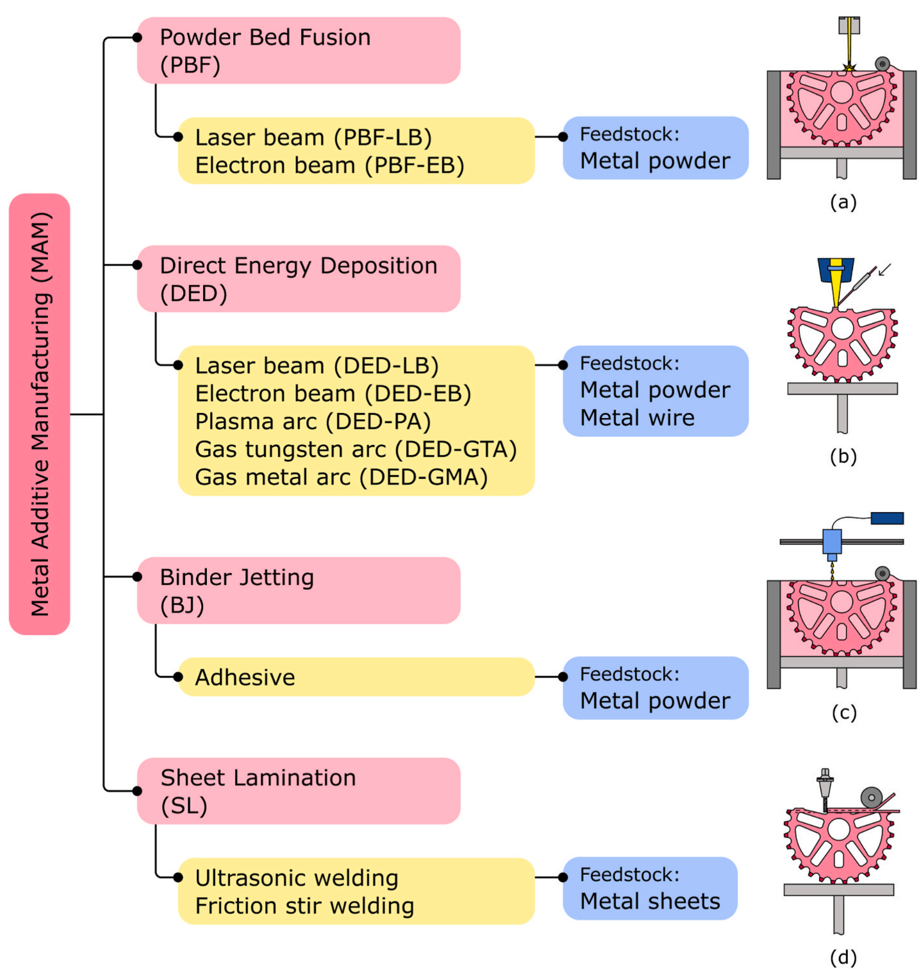

Fig. 1. Classification of metal additive manufacturing (MAM) processes with schematic representations of (a) powder bed fusion with electron beam (PBF-EB), (b) direct energy deposition with laser beam (DED-LB), (c) binder jetting (BJ), and (d) sheet lamination (SL) with ultrasonic welding.

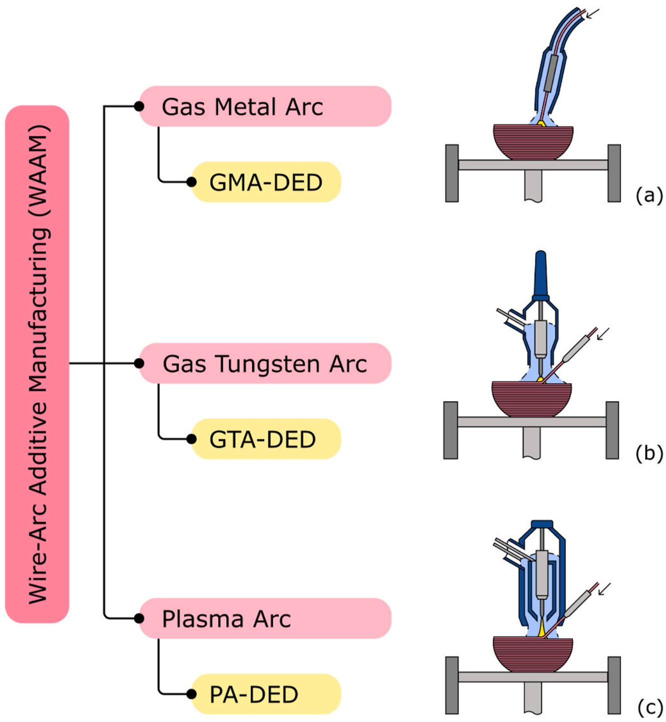

Fig. 3. Classification of wire-arc additive manufacturing (WAAM) processes considering the heat source with schematic representations of (a) gas metal arc DED (GMA-DED), (b) gas tungsten arc DED (GTA-DED), and (c) plasma arc DED (PA-DED).

Table 1
Main aspects covered in WAAM state-of-the-art reviews.

Working principles	Ding et al. (2015), Derekar (2018), Wu et al. (2018), Rodrigues et al. (2019) Savyasachi et al. (2020), Jin et al. (2020), Liu et al. (2020), Pattanayak and Sahoo (2021), Raut and Taiwade (2021), Singh and Khanna (2021), Treutler and Wesling (2021), Li et al. (2022), Tomar et al. (2022)
Process parameters	Ding et al. (2015), Derekar (2018), Wu et al. (2018), Rodrigues et al. (2019), Jin et al. (2020), Liu et al. (2020), Pattanayak and Sahoo (2021), Raut and Taiwade (2021), Singh and Khanna (2021), Treutler and Wesling (2021), Li et al. (2022), Tomar et al. (2022)
Equipment	Rodrigues et al. (2019), Jin et al. (2020), Liu et al. (2020), Pattanayak and Sahoo (2021), Raut and Taiwade (2021), Singh and Khanna (2021), Li et al. (2022)
Control and sensing	Liu et al. (2020), Pattanayak and Sahoo (2021), Raut and Taiwade (2021), Treutler and Wesling (2021), Singh and Khanna (2021), Li et al. (2022), Tomar et al. (2022)
Materials	Ding et al. (2015), Derekar (2018), Wu et al. (2018), Rodrigues et al. (2019), Savyasachi et al. (2020), Jin et al. (2020), Liu et al. (2020), Pattanayak and Sahoo (2021), Raut and Taiwade (2021), Singh and Khanna (2021), Treutler and Wesling (2021), Tomar et al. (2022)
Microstructure	Derekar (2018), Wu et al. (2018), Rodrigues et al. (2019), Liu et al. (2020), Jin et al. (2020), Savyasachi et al. (2020), Pattanayak and Sahoo (2021), Raut and Taiwade (2021), Treutler and Wesling (2021), Tomar et al. (2022)
Defects	Ding et al. (2015), Derekar (2018), Wu et al. (2018), Rodrigues et al. (2019), Jin et al. (2020), Liu et al. (2020), Pattanayak and Sahoo (2021), Raut and Taiwade (2021), Singh and Khanna (2021), Li et al. (2022), Tomar et al. (2022)
In and out-process treatments	Derekar (2018), Wu et al. (2018), Rodrigues et al. (2019), Pattanayak and Sahoo (2021), Raut and Taiwade (2021), Singh and Khanna (2021), Treutler and Wesling (2021), Tomar et al. (2022)
Applications	Ding et al. (2015), Rodrigues et al. (2019), Liu et al. (2020), Pattanayak and Sahoo (2021), Treutler and Wesling (2021), Li et al. (2022), Tomar et al. (2022)

the deposited material to the one of the finished metal part approximately equal to 1.2, which are far below the typical values of 10 to 20 for parts machined out of forged preforms.

In recent years the growing interest in WAAM stimulated the publication of several state-of-the-art review papers covering different aspects of the process such as the working principle, process parameters, equipment, control and sensing, materials, microstructure, defects, in and out-process treatments, and applications. Table 1 provides a summary of these efforts showing which aspects are covered in the different state-of-the-art reviews.

One conclusion that can be drawn from Table 1 is that only the accumulation of new developments in WAAM, which will naturally occur in the coming years, or any disruptive technological breakthrough justifies the necessity of additional state-of-the-art reviews. Nevertheless, there is still a topic – modelling – not included in Table 1, which has little or no attention at all from WAAM state-of-the-art reviews. In fact, most of the papers ignore the topic, which is of paramount importance to obtain a better knowledge of the physics of the process, to eliminate the trial-and-error selection of operating parameters, to predict and avoid the occurrence of defects or undesirable microstructures, to improve the mechanical strength of the parts and to foster the development of WAAM to new materials and applications.

Under these circumstances, the aim and objective of this paper is to provide a review of modelling of WAAM. In contrast to a paper recently published by Liu et al. (2021) that gives special emphasis to models for heat and mass transfer and microstructure evolution at meso and micro-scale levels, this paper will draw from the technology and physics of WAAM to focus on macro-scale level modelling using the finite element method.

The paper is organized into five different sections including this introduction with a brief classification and description of the main technologies used in metal additive manufacturing (MAM) and of the main processes in wire-arc additive manufacturing (WAAM). Section 2 presents the working principles of WAAM and systematizes its main operating parameters due to their relevance to the development and application of simulative models. Section 3 distinguishes between micro, meso, and macro-scale modelling explaining their aims and objectives. Section 4 is focused on macro-scale modelling and covers analytical, statistical, machine learning and finite element analysis. Special emphasis is given to finite element analysis by providing a detailed analysis of the pre-processing requirements, solution techniques and results that are commonly found in publications. Finally, Section 5 provides future research directions and conclusions.

2. WAAM technology

Gas metal arc direct energy deposition (GMA-DED) is the most widespread process utilized in WAAM (Fig. 4). In this process, an electric arc is established between the tip of a consumable wire (electrode) and the metal part, under the protection of inert or active shielding gases. The wire is fed automatically from a continuous spool through a nozzle and fused to create molten droplets that are detached and impinged into the pool of molten material created by the arc.

The depth of the melt pool is determined by the supplied power $\dot{Q}$ and travel speed v_t of the torch (moving heat source), and the specific heat c and thermal conductivity k of the wire material being deposited. The supplied power $\dot{Q}$, travel speed v_t, wire feedstock diameter d_f and wire feed rate v_f affect the amount of material transferred into the melt pool and, therefore, the volume of material that is fused and deposited in the part (Messler, 2004).

Slow-moving and fast-moving melt pools experience different thermal cycles and therefore give rise to different microstructures and mechanical properties of the deposited materials (Pragana et al., 2021a).

Knowledge and control of the main process parameters are,

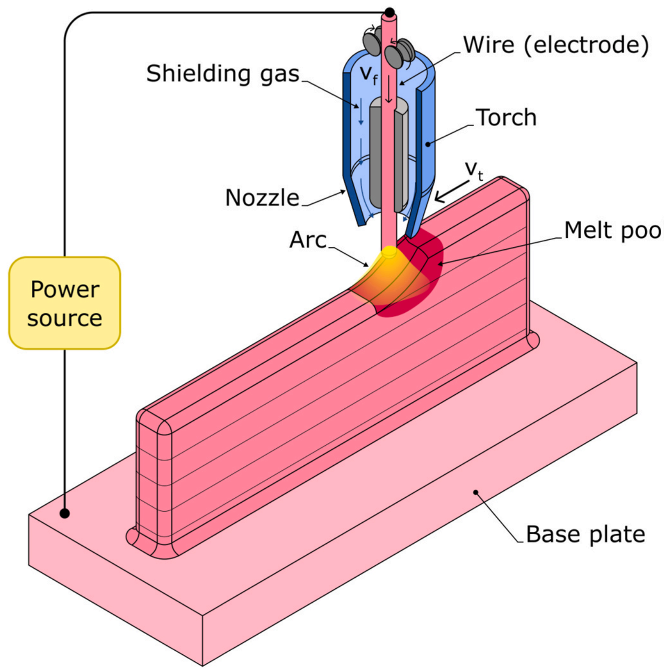

Fig. 4. The working principle of WAAM (GMA-DED) with main terminology.

therefore, of paramount importance because, as shown in Fig. 5a, the microstructures of metal parts produced by WAAM have strong crystallographic textures characterized by dendritic growth of columnar grains with primary arms preferentially aligned with the highest temperature gradient (building direction) (Pragana et al., 2022).

The dendritic growth of columnar grains justifies the anisotropic mechanical behaviour of the additively deposited tubes that is shown in Fig. 5c. As seen in the figure, the results obtained from conventional and ring hoop tension tests carried out in specimens cut out from the additively deposited tubular parts, at room temperature, show significant variations of the stress-strain response along different directions. This problem does not occur in commercial wrought tubes of the same material, whose microstructure is basically equiaxial with stable polygonal grain features (Fig. 5b).

The working principles of the other two WAAM-based processes included in Fig. 3 - gas tungsten arc direct energy deposition (GTA-DED) (Baufeld et al., 2010) and plasma arc direct energy deposition (PA-DED) (Martina et al., 2012) - make use of electric arcs that are formed between a non-consumable electrode (typically made of tungsten) and the metal part.

The main difference to GMA-DED is that usually there are no molten droplets transferred across the arc because the wire feedstock is not supplied through the nozzle, but directly to the melt pool through a wire feeding unit. Few exceptions can be found on compulsively constricted PA-DED, in which an indirect arc is ignited between a tungsten electrode and the wire feedstock inside a very confined nozzle. This diminishes material spatter and the amount of particle and fume generation (Jia et al., 2020).

In what concerns the main differences between GTA-DED and PA-DED one may refer the fact that the electric arc in PA-DED has greater energy concentration, better stability, and less thermal distortion than in GTA-DED (Feng et al., 2018). This explains the reason why the

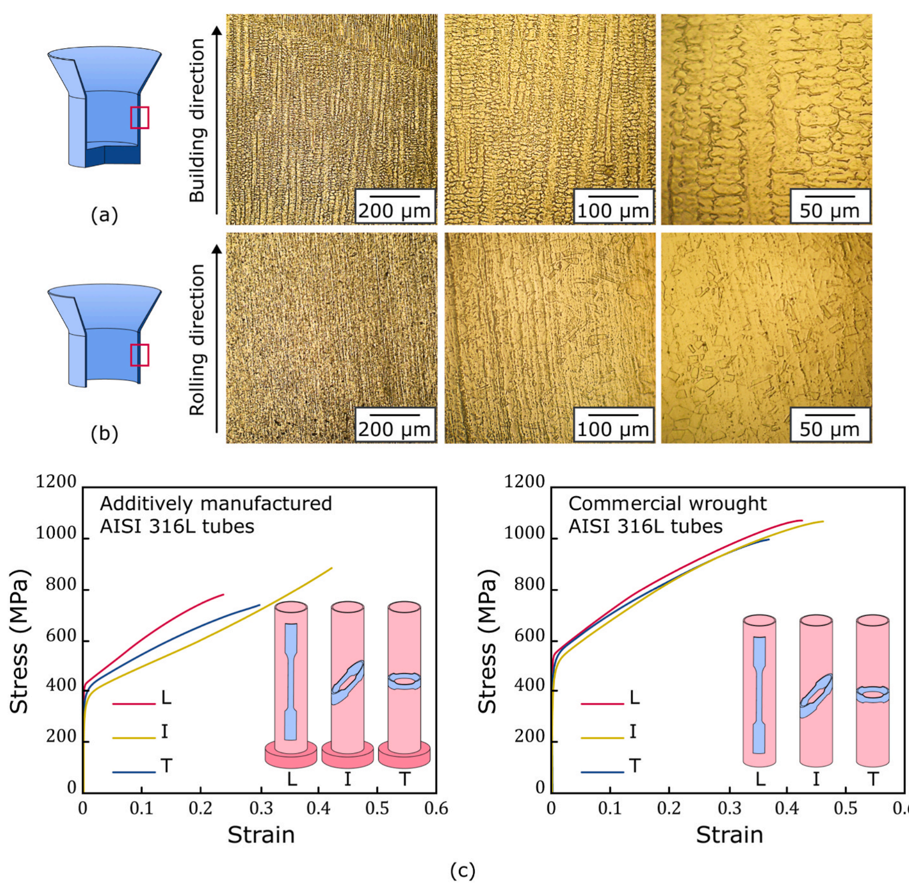

Fig. 5. Influence of WAAM on microstructure and mechanical behaviour of metal parts. Microstructures of metallographic samples taken from (a) additively deposited and (b) commercial wrought AISI 316L stainless steel tubes. (c) Stress-strain curves obtained from test specimens cut out from additively deposited (left) and commercial wrought (right) AISI 316L stainless steel tubes in longitudinal (L), inclined (I) and transversal (T) directions (adapted from Pragana et al., 2022).

deposition rates of PA-DED are higher than those in GTA-DED, and the fact that PA-DED is the only electric arc-based MAM process that can use powder as feedstock (Zhang et al., 2003).

Still, the modelling challenges of GTA-DED and PA-DED are like those of GMA-DED, which basically consist of identifying and incorporating their process parameters (Fig. 6) into macro, meso and micro-scale level digital twins designed to accurately reflect the physical process. Modelling will be used to tune the process parameters in order to ensure fast built times and improve the surface finish, dimensional accuracy, microstructure and mechanical performance of the constructed metal parts. The optimization of the process parameters, if proven of value and effective, will lead to the elimination of in and out-process treatments and to an efficient use of wire feedstock by reducing the machining operations that are needed at the end of WAAM to meet the part specifications.

3. Modelling of WAAM

WAAM can be described at three different scales: macro, meso, and micro (Fig. 7). The description at macro-scale (Fig. 7a) is performed by means of thermo-mechanical coupled models that replace the torch and electric arc by a heat source model (e.g., Goldak et al., 1984) to obtain the temperature history as a function of time as well as the displacements, strains, and stresses. This information allows predicting the cooling and solidification rates, microstructure, residual stresses, and distortions of the metal parts.

Macro-scale description of WAAM using thermo-mechanical coupled models can effectively be used to identify and optimize process parameters as claimed by Montevecchi et al. (2016), Graf et al. (2018), Ahmad et al. (2020), and Hackenhaar et al. (2020), among other researchers.

Temperature history as a function of time, temperature peaks, temperature gradients, and cooling and solidification rates are the main factors influencing the microstructure. Therefore, phase transformations and grain growth in WAAM can be predicted by coupling temperature history resulting from the macro-scale modelling with time dependent metallurgical equations built upon hardenability algorithms like those comprehensively exposed and applied to the welding processes of low alloy steels by Watt et al. (1988).

A major drawback of macro-scale models is their inability to describe the heat transferred in the arc and the formation, detachment and impingent of the molten droplets from the arc into the melt pool. This is a fluid flow and heat transfer phenomenon that must be analysed at meso-scale level (Fig. 7b) by means of complex multi-physics models encompassing the four different states of matter (plasma, gas, liquid and solid) and their interactions. Examples of meso-scale modelling of WAAM are reported in the literature by Fan and Kovacevic (1999), Wang et al. (2003) and Cadiou et al. (2020).

A unified model proposed by Hu and Tsai (2007b, 2007a) to account for all these phenomena allows concluding that the transfer of droplets and the deformed melt pool surfaces have a significant influence on the transient distributions of current density, arc temperature and arc pressure, which are normally assumed to be constant Gaussian profiles in the heat source models that are used at macro-scale level. However, the extension of the applicability domain of these complex multi-physics meso-scale models requires coupling the fundamental equations

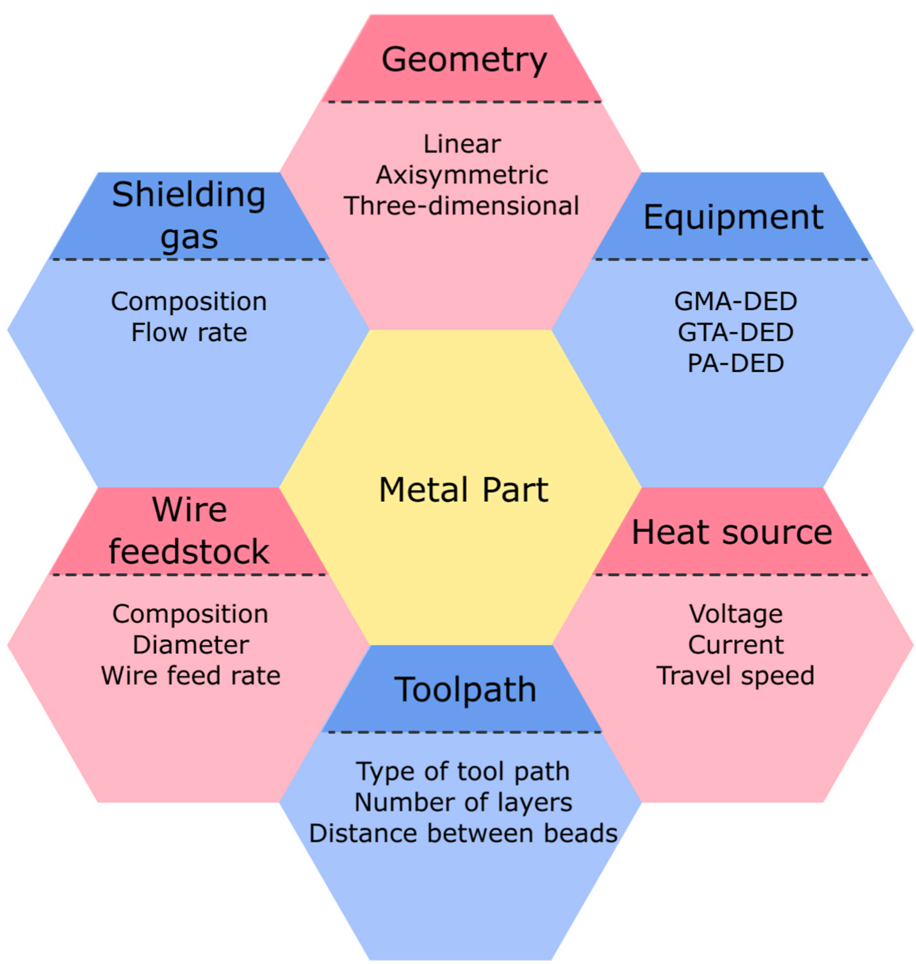

Fig. 6. The main process parameters in WAAM.

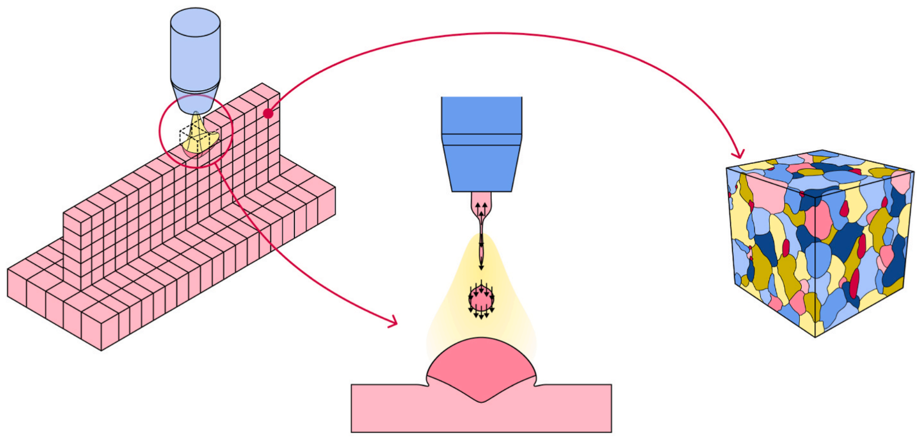

Fig. 7. WAAM modelling at the three different scales: (a) macro, (b) meso and (c) micro.

governing the conservation of mass (1), momentum (2) and energy (3), and the current continuity equation (4) to real metal part sizes,

$$\frac{\partial \rho}{\partial t} + \nabla \bullet (\rho \boldsymbol{v}) = 0 \quad (1)$$

$$\rho\left(\frac{\partial \boldsymbol{v}}{\partial t} + \boldsymbol{v} \bullet \nabla \boldsymbol{v}\right) = -\nabla p + \mu \nabla^2 \boldsymbol{v} + \frac{1}{3}\mu \nabla(\nabla \bullet \boldsymbol{v}) + \rho \boldsymbol{f} \quad (2)$$

$$\rho \dot{w} = \boldsymbol{\sigma} : \boldsymbol{D} + \dot{q} - \nabla \boldsymbol{q} \quad (3)$$

$$\nabla^2 \Phi + \Sigma = 0 \quad (4)$$

In the above equations, ρ is the density, μ is the viscosity, t is time, $\boldsymbol{v}$ is the velocity vector, p is the pressure, $\boldsymbol{f}$ is the internal forces (forces per unit of mass), $\dot{w}$ is the internal energy rate per unit of mass, $\boldsymbol{\sigma}$ is the Cauchy stress tensor, $\boldsymbol{D}$ is the rate of deformation tensor, $\dot{q}$ is the heat generation rate per unit of volume, $\boldsymbol{q}$ is the heat flux vector, Φ is the electric potential and Σ is the electric potential source.

Besides the complexity of coupling equations (1) to (4), there is the problem of the time duration of the meso-scale phenomena, which are very small compared to the building times of metal parts at macro-scale level. This constrains multi-scale level applicability and leads to inadmissible CPU requirements.

Phase transformations and microstructure formation can be described by means of micro-scale models (Liu et al., 2021) instead of time dependent metallurgical equations built upon hardenability algorithms. The micro-scale models are generally linked to a specific location on the macro-scale model (e.g., a nodal point of the finite element mesh) and act as a representative volume element (RVE) (Fig. 7c). Phase field thermodynamic-based models for solving interfacial problems are then used to simulate solidification, grain growth and phase transformations in the deposited metal part (Provatas and Elder, 2010).

Alternative approaches based on Monte Carlo and cellular automata randomness computational algorithms can also be used to obtain the same information (Yang et al., 2011). However, the utilization of RVE's requiring exchange of information between the macro and micro-scale models (in both ways) to solve the thermal cycle of the build metal part while capturing the evolution of its microstructure has strong limitations in modelling real manufacturing timescales.

4. Macro-scale modelling of WAAM

4.1. Analytical modelling

The foundations of the analytical modelling of WAAM are the development and application of the heat transfer equation for moving heat sources in arc welding (Rosenthal, 1946),

$$T(\xi, y, z) - T_0 = \frac{\dot{Q}}{2\pi k r} exp^{\left(-\frac{\rho c v_t}{2k}(r+\xi)\right)} \quad (5)$$

In the above equation, T_0 is the ambient temperature, $\dot{Q}$ is the heat source power, $\xi = x - v_t t$ is the linear moving coordinate, where v_t is the travel speed of the heat source and t is time, k is the thermal conductivity, ρ is the density, c is the specific heat, and $\boldsymbol{r} = \sqrt{\xi^2 + y^2 + z^2}$ is the radial distance to the moving heat source.

Rosenthal's equation (5) includes a series of assumptions such as: (i) the specific heat c, density ρ and thermal conductivity k are independent from temperature, (ii) the latent heat of the liquidus-solidus phase transformation is ignored, (iii) the heat losses by radiation and convection to the environment are neglected and (iv) the heat source is pointwise. Despite these assumptions, equation (5) was the first step towards prediction of temperature history as a function of time, temperature gradients, and cooling and solidification rates.

The use of equation (5) to model the thermal cycle and the geometry of the melt pool in WAAM is constrained by three major problems. Firstly, the estimate of infinite temperatures at the origin of the moving heat source (Fig. 8).

Secondly, the assumption of conduction heat transfer while neglecting the dominant convection heat transfer due to fluid flow in the melt pool. These two problems, which are common to welding, lead to analytical predictions of the melt pool dimensions that are different from those experimentally measured (Nasiri and Enzinger, 2019). The third problem, illustrated in Fig. 9, suggests that the differences in the melt pool cross sections of arc welding and WAAM should inevitably give rise to differences in the melting efficiency of both processes due to differences in the heat transferred to the solid metal and lost to the environment (Mohebbi et al., 2020). In particular, the approximate semi-infinite plate heat transfer conditions of arc welding are different from the approximate one-dimensional heat transfer conditions of material deposition in WAAM.

As a result of the above-mentioned problems, recent years saw the modification of equation (5) to provide better description of the melting interface (Nasiri and Enzinger, 2019) and the development of new analytical models to calculate the power of the heat source and the geometry of the melt pool for various DED processes with wire feedstock.

Pinkerton and Li (2004), for example, proposed a model derived from equation (5) that performs mass and energy balances based in one-dimensional heat conduction to the solid metal. The travel speed v_t of the heat source is taken into consideration and the melt pool boundaries are assumed as arcs of a circle rather than ellipses to account

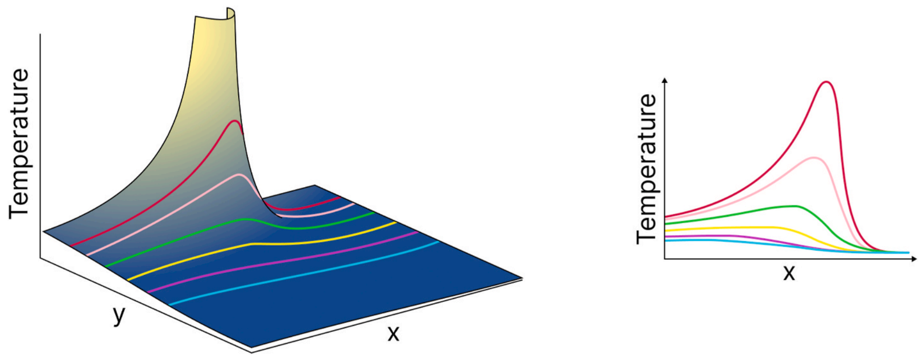

Fig. 8. Schematic representation of temperature isotherms for a moving point heat source.

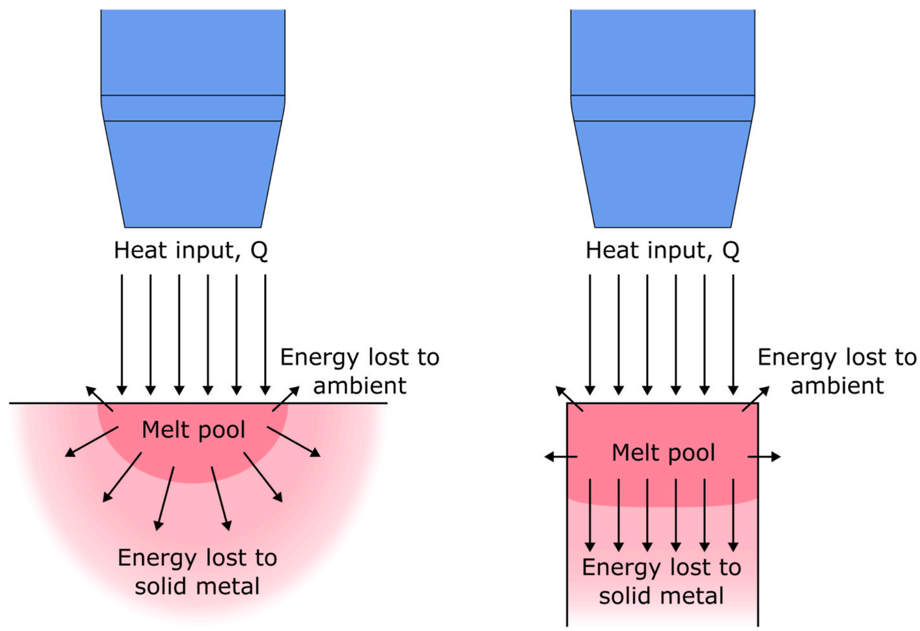

Fig. 9. Schematic representation of the melt pool cross-section with indication of the heat losses to the solid metal and to the environment in case of (a) arc welding and (b) WAAM. (Adapted from Mohebbi et al., 2020).

for surface tension. The model was successfully applied in DED-LB.

Another analytical model due to Ríos et al. (2018) combined a modified version of equation (5), which allows calculating the heat source power from the melt pool dimensions (Wells, 1952), with a capillarity analysis of the geometry of deposits. The model was successfully applied in WAAM to predict the influence of different process parameters on the geometry of the deposited material.

Several other researchers could have been cited, but despite the ability of analytical models to predict temperature history as a function of time and the cooling and solidification rates that are needed to predict microstructure, residual stresses and distortions, their use is limited to simple heat source models, to material properties independent from temperature and to material depositions along linear paths. Solutions for arbitrary paths, considering temperature dependent material properties and more complex heat source models (e.g., Gaussian distributed) require the utilization of other types of models.

4.2. Statistical and machine learning models

The use of statistics in WAAM serves two main objectives: (i) to find significance on the relationships between input and output data and/or (ii) to create models that can predict or optimize output data from input data. As an example of the first objective, one can refer the work of Dinovitzer et al. (2019), who used analysis of variance (ANOVA) in WAAM (GTA-DED) to conclude that: (i) the bead height increases linearly with wire feed rate, (ii) the depth of the melt pool and roughness are independent of wire feed rate, (iii) the bead width decreases with travel speed and (iv) the travel speed and current affect heat input inversely and, therefore, give rise to opposite relationships between input and output data.

The work of Martina et al. (2012) fits into the above-mentioned second objective because it consists of the development of a statistical model that enables the selection of process parameters (e.g., travel speed of the heat source and input current) to maximize the layer height and the deposition rate for a given wall width in WAAM (PA-DED).

In contrast to statistical models, machine learning models are designed to provide the most possible accurate predictions. They are based on computing techniques such as artificial neural networks (ANN) that are built upon the different connections between input and output data. Ding et al. (2016), for example, established a relationship between single bead geometry and process parameters through an ANN in which the input layer receives wire feed rate v_f and travel speed v_t data, and the output layer produces results for the bead width w and height h (Fig. 10). Results in WAAM showed that the machine learning model could accurately predict the bead geometry and, therefore, be used to determine the optimum process operating conditions.

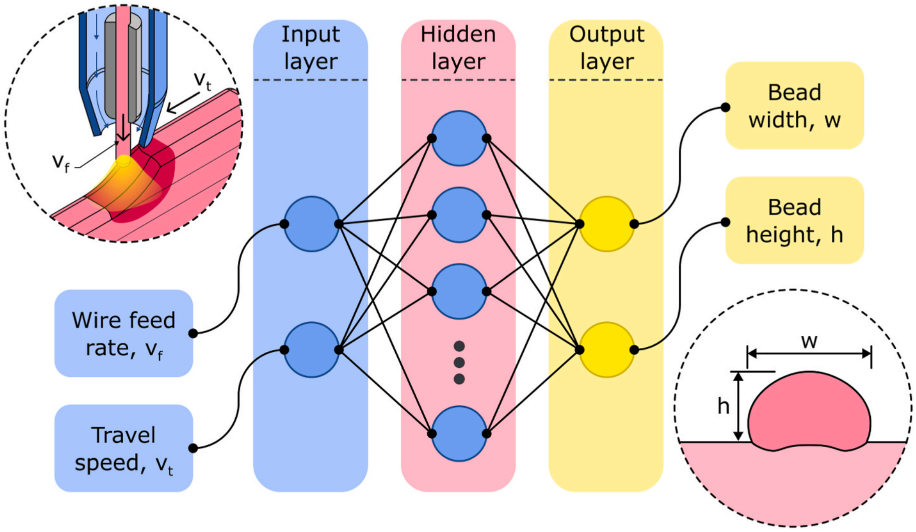

Fig. 10. Schematic representation of the artificial neural network that was used to predict a single bead geometry in WAAM (adapted from Ding et al., 2016).

Li et al. (2018) created an ANN in which the input layer brings data on the bead width w, bead height h, and centre distance of adjacent deposition paths d_p into the model for further processing by a hidden layer and produce the offset distance d_o in the output layer (Fig. 11). This specific ANN was embedded in a closed-loop iteration algorithm to determine the optimal value of the centre distance of adjacent deposition paths and allow better control of the surface unevenness of multi-bead layers.

Chowdhury (2013) focused on the defects of the metal parts and constructed an ANN to help countering thermal induced deformations by receiving and processing data from deformed metal parts.

Several other examples could have been provided, but the main question related to machine learning models is to understand their advantages and disadvantages in WAAM. In what concerns the advantages: (i) they can easily identify trends and patterns that would not be evident to researchers and engineers by handling and reviewing large volumes

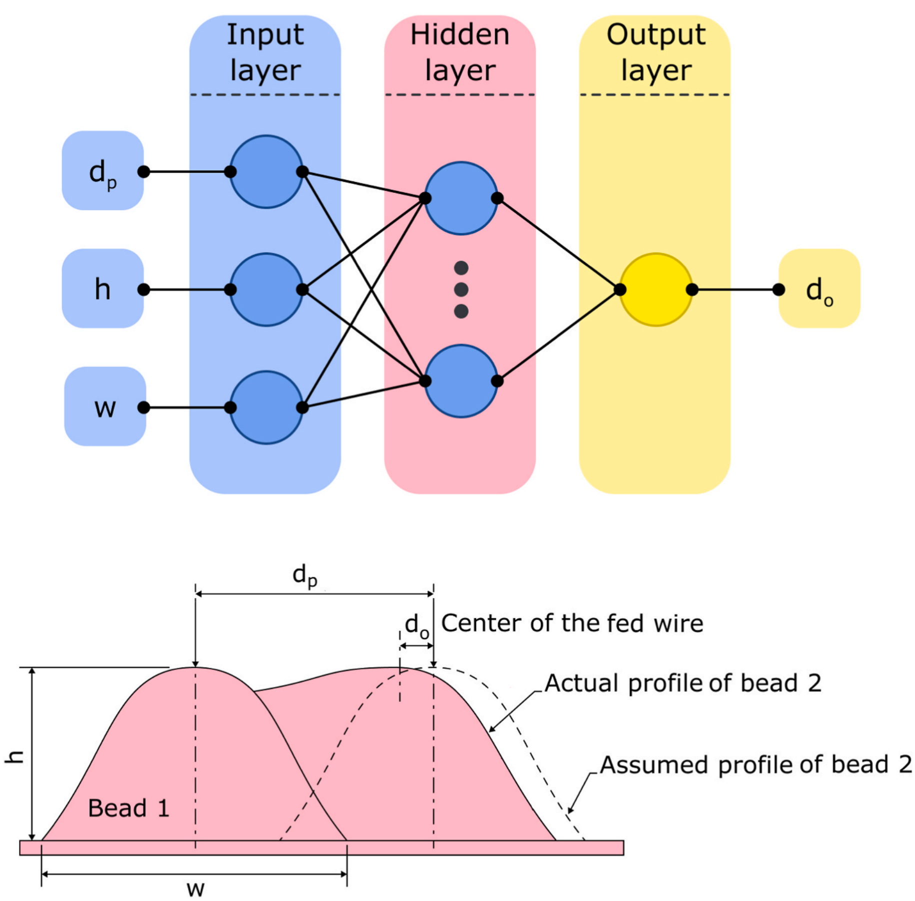

Fig. 11. Schematic representation of the artificial neural network that was used to predict the offset distance in adjacent deposition paths (adapted from Li et al., 2018).

of data, (ii) they can enhance this capability through continuous improvement as the amount of data grows and (iii) they can cover many different aspects of the process from the relation between operating parameters and melt pool geometry to the connection between operating parameters and residual stresses, distortions, and microstructures, among other aptitudes.

The main drawbacks of machine learning models in WAAM are related (i) to the necessity of users performing cautious interpretation of the results to prevent miscalculations and errors and (ii) to the significant amount of data, time and resources that are needed to train the models. This second problem often requires combination of experimental data with numerical simulation predictions obtained by e.g., finite element modelling.

4.3. Finite element modelling

4.3.1. Introduction

Macro-scale finite element modelling of WAAM by means of commercial or self-developed software (Lavery et al., 2014), has roots in the pioneering three-dimensional computational welding simulations that were carried out in the late 1980's and early 1990's by Tekriwal and Mazumder (1988) and Karlsson and Josefson (1990). The book of Goldak and Akhlaghi (2005) provides a comprehensive exposure and a historical perspective of the major contributions and developments by different researchers in the field.

Finite element computer programs utilized at macro-scale level make use of asymmetric Gaussian distributed heat source models, like the double-ellipsoidal moving heat source of Goldak et al. (1984), to account for the total power transferred to the filler and base (deposited and substrate) materials. The use of heat source models circumvents the use of complex numerical simulations of the heat and mass transfer in the electric arc and of the heat transfer due to fluid flow in the melt pool, which are the core of meso-scale finite element modelling.

Fig. 12 provides a glimpse of a typical finite element environment to model WAAM at macro-scale level. The first stage (pre-processing) consists of supplying all the necessary information (input data) for running the programs:

a) Geometry of the metal part – discretization of the final geometry of the metal part by means of three-dimensional elements,
b) Heat source – heat source model and amount of power transferred to the filler and base materials,
c) Boundary conditions - size, travel speed and moving path of the heat source, identification of the mechanical and heat transfer boundary conditions, and selection of the numerical technique utilized to replicate material deposition, layer-by-layer,
d) Analysis type - decision on the type of simulation to be performed and on the type of thermo-mechanical coupling (coupled vs. staggered),
e) Material data - supply of the temperature dependent material properties,
f) Numerical parameters - choice of time increment and convergence conditions, among other parameters.

The finite element computer programs for the macro-scale simulation of WAAM combine the solution of the heat transfer equation,

$$k\nabla^2 T - \rho c \frac{\partial T}{\partial t} + \dot{Q} = 0 \tag{6}$$

where k is the thermal conductivity, ρ is the density, c is the specific heat, and $\dot{Q}$ is the heat generation rate, with the solution of the quasi-static equilibrium equations in the current configuration of the metal part (in the absence of body forces),

$$\frac{\partial \sigma_{ij}}{\partial x_j} = 0 \tag{7}$$

where σ_{ij} is the Cauchy stress tensor and x_j is an arbitrary position of the metal part at the current instant of time.

The thermo-mechanical solution requires the metal part geometry to be discretized into a mesh of three-dimensional elements, linked by nodes, so that calculations resulting from equations (6) and (7) at element level are assembled into a global system of equations and solved for the entire metal part. The calculations are carried out incrementally (through subdivision of the process time into a series of time increments), and iteratively within a time increment due to the following three main sources of non-linearity:

a) Material nonlinearity,
b) Changing boundary conditions,
c) Geometric nonlinearities

Material nonlinearity is associated with the temperature dependence of the material properties (e.g., thermal conductivity, density, specific heat capacity and elasticity modulus, among others). The thermal strains and the non-linear stress-strain material behaviour in the plastic regime (flow curve) are also sources of material nonlinearity.

Changing boundary conditions are mainly due to the activation of

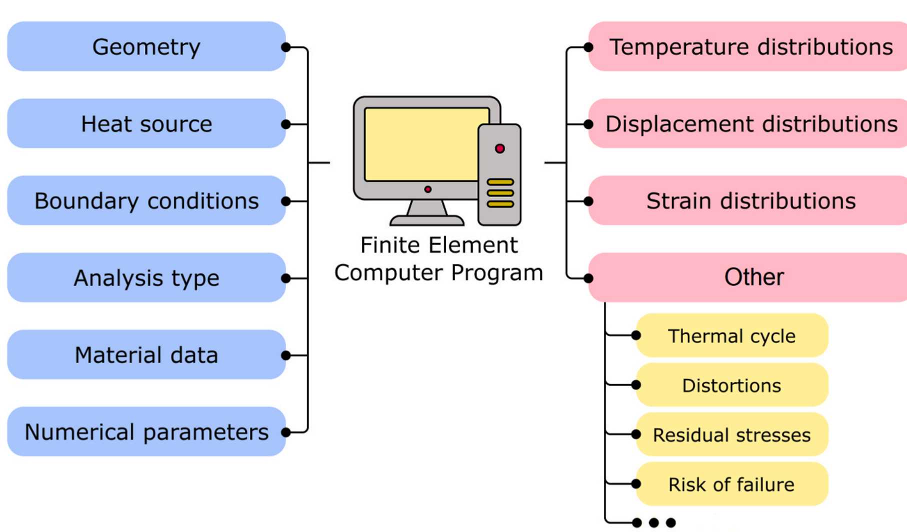

Fig. 12. Finite element modelling environment in the macro-scale simulation of WAAM.

new mesh elements with specific thermal conditions resulting from the travel speed of the heat source along the moving path.

Geometric nonlinearity is related to the distortions induced by the thermal strains upon removing the clamps from the constructed metal parts.

Because finite element calculations are carried out in a mesh, rather than in the entire metal part, results generally require interpolation between nodes to produce the output data. The latter consists of temperature, displacement, strain, and stress distributions and may be directly used in 'post-processing' or further worked to provide information on the thermal cycle, local peak temperatures (hot spots), overheating and lack of fusion, risk of failure, residual stresses and distortions, and to optimize the building construction strategies of the metal parts.

Several examples of macro-scale modelling of WAAM using commercial software such as ABAQUS (e.g., Saadatmand and Talemi, 2020), ANSYS (e.g., Srivastava et al., 2022), MSC Marc (e.g., Xiong et al., 2017), LS-DYNA (e.g., Israr et al., 2021), SIMUFACT (e.g., OyamaDiplas et al., 2019), and open-source (e.g., Cambon et al., 2020) or in-house software (e.g., Nijhuis et al., 2021) are given in the literature. Comparisons between commercial and open-source software are also available (e.g., Bauer et al., 2021).

4.3.2. Geometry of the metal part

Discretization of the substrate (base plate) and deposited materials into elements is carried out at the pre-processing stage and requires generating all the elements of the base plate and of the final deposited metal part. The elements of the base plate will be active from the beginning of the simulation, while those of the deposited material will be activated gradually as the heat sources move along its path, layer-by-layer. Two different approaches are commonly used to build the finite element models and perform the activation process ('element birth'), as will be discussed in the subsection entitled 'Boundary conditions'.

Hexahedral elements are the most used finite elements in WAAM because most of the applications published in the literature refer to linear, multi-layer, depositions (e.g., Montevecchi et al., 2017; Tangestani et al., 2020; Nijhuis et al., 2021). However, there are some publications where discretization of the base plate and deposited material is performed by means of tetrahedral elements (Bauer et al., 2021).

Typical hexahedral element meshes can be structured with all the interior nodes having an equal valence (i.e., equal number of adjacent elements), or unstructured with interior nodes having arbitrary valences resulting from non-conformal discretization of the base plate and deposited materials. The choice between structured and unstructured meshes is a recurring discussion in mesh generation, but what really matters in the end is the adequacy of a mesh to accurately perform the calculation of the field variables with the smallest possible CPU requirements.

Structured meshes can be regular with elements of equal size in both the base plate and deposited material (Fig. 13a) or biased with elements progressively increasing or decreasing in size along specific directions or locations (Fig. 13b). The use of structured meshes with elements of equal size requires the utilization of very large meshes to ensure good quality of the numerical predictions. This leads to many degrees of freedom and to very large stiffness matrices that substantially increase the memory and CPU time requirements.

Structured biased meshes alleviate the above-mentioned problem by increasing the element size in the base plate with the distance from the deposited material (e.g., Mughal et al., 2006). This reduces the total number of degrees of freedom without losing accuracy and efficiency of the calculations in the regions of higher temperature gradients and stress concentrations.

The unstructured meshes utilized in WAAM are usually of two different types. One type involves the insertion of proper transition templates in different locations (e.g., near base plate to deposited material transitions) to satisfy the connectivity requirements (Fig. 13c). In this case, relaxation of the node valence allows creating meshes with a smaller number of elements, in which element density is locally increased in specific regions of the parts where the gradients of the field variables are higher (e.g., Tangestani et al., 2020; Nijhuis et al., 2021).

The other, more general type involves subdividing the entire volume into blocks with different mesh sizes and treating their interfaces as contact between deformable objects (Zavarise and Wriggers, 1998) (Fig. 13d). Montevecchi et al. (2017), Graf et al. (2018) and Hackenhaar et al. (2020) provide examples in which the meshes were built from multiple objects with different element sizes.

A typical finite element procedure to handle the meshes built from multiple objects consists of automatically creating contact pairs between the nodes of one object and the element surfaces of the other object to determine the new contact surface after a time increment Δt, whilst satisfying the mechanical and thermal governing equations and preventing overlapping between the objects. This approach is the most versatile to generate meshes with different element sizes. However, it increases the number of off-diagonal blocks relating nodes to each other in the thermal and mechanical stiffness matrices, leading to additional memory and computational time requirements to solve the systems of equations in each iteration (Nielsen and Martins, 2021).

Another topic related to meshes in some WAAM publications (e.g., Denlinger et al., 2014, and Jayanath and Achuthan, 2018) is the utilization of adaptive remeshing techniques in a layer-by-layer basis to perform mesh coarsening and progressive merging of the elements located in the lower layers of the deposited material (Fig. 13e). This approach enables local control and prevention of an overwhelming number of elements. However, it requires implementation of renumbering optimization algorithms along with numerical procedures for the automatic transfer of the time-integrated variables, such as temperature and strain, from the previous to the coarsened meshes.

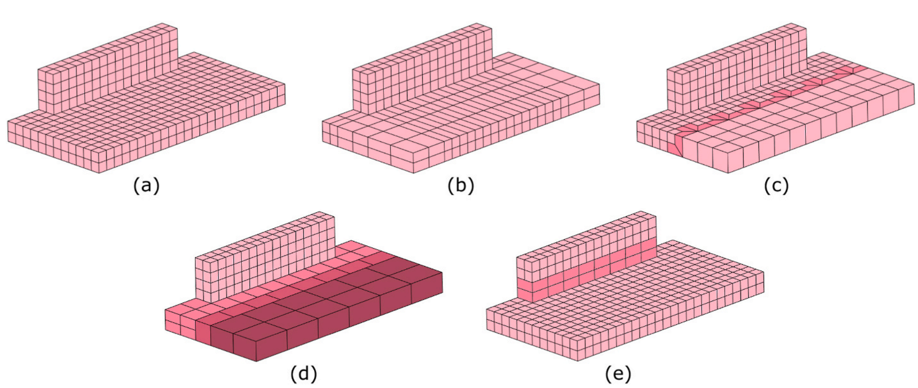

Fig. 13. Different types of meshes utilized in WAAM: (a) regular mesh, (b) structured biased mesh, (c) unstructured mesh with transition templates, (d) unstructured mesh with multiple deformable objects in contact, and (e) layer-by-layer mesh coarsening of the deposited material.

4.3.3. Heat source

The double ellipsoid heat source model proposed by Goldak et al. (1984) is commonly used in the finite element modelling of WAAM and followed earlier models based on disc (Krutz and Segerlind, 1976), hemispheric and single ellipsoid shapes that were also aimed at replicating the distribution of the thermal energy supplied to a workpiece during welding.

The double ellipsoid model is defined by means of two geometric parameters that represent the half-width b and depth d of the welding pool and by two other geometric parameters that define the maximum distances a_f and a_r between the broadest spots of the pool to the melt front (x-positive) and rear (or, solidification front, x-negative). The values of b and d may be taken from a cross-section of the deposited material while $a_f \cong 0.5b$ and $a_r \cong 2b$ in the absence of experimental data (Goldak et al., 1984).

The four parameters $a_{f,r}$, b, and d are the semi-axis of two ellipsoids (front f and rear r) centred in the origin of the frame of reference xyz and allow writing the power density $\dot{q}$ supplied by the moving heat source as the following asymmetric Gaussian distribution (Fig. 14a),

$$\dot{q} = \frac{6\sqrt{3}\dot{Q}f_{f,r}}{\pi\sqrt{\pi}a_{f,r}bd} exp\left\{-3\left(\frac{x^2}{a_{f,r}^2}+\frac{y^2}{b^2}+\frac{z^2}{d^2}\right)\right\} \tag{8}$$

In the above equation, $\dot{Q} = \eta UI$ is the total input power of the heat source, where η is the arc efficiency, U is the voltage and I is the electric current. The factors f_f and f_r are the fractions of the thermal energy transferred to the front and rear ellipsoids (with, $f_f + f_r = 2$).

The double ellipsoid heat source model spreads the thermal energy through the melt pool volume more accurately than others and is commonly used in finite element modelling of WAAM. Examples of application are found in the work of Ding et al. (2014), Graf et al. (2018), Ahmad et al. (2020) and Ling et al. (2021), among others.

However, as in computational welding, the precision of the double ellipsoid heat source model is known to be less satisfying in the melt pool. In some cases, the calculated temperatures can go above the evaporation temperature and require modification of the intensity parameter in equation (8), by using 1 or 2, instead of 3 (Mokrov et al., 2019).

Montevecchi et al. (2016) analysed these difficulties and showed that the thermal energy transmitted to the metal part depends upon the relative position between the heat source frame of reference and the base material. The melt pool temperatures can overshoot in case the origin of the heat source frame of reference is positioned on the top surface of the base material and the base material temperatures can undershoot in case the origin of the heat source frame of reference is positioned on top of the filler material.

The solution proposed by Montevecchi et al. (2016) is three-fold (Fig. 14b). Firstly, to account for a 50% distribution of heat input Q between the base Q_b and filler Q_w materials. Secondly, to use a double ellipsoid power density function $\dot{q}_b$ for the base material by replacing $\dot{Q}$ with $\dot{Q}_b$ in equation (8). Thirdly, to use a constant power density distribution $\dot{q}_w$ for the filler material,

$$\dot{q}_w = \frac{\dot{Q}_w}{V_{el}} \tag{9}$$

where $V_{el} = lwh$ is the volume of each deposited droplet (the currently heated filler material of the model) assumed as a box with length l, width w and height h. In computational terms, this means that $\dot{q}_w$ should be applied only to the elements of the mesh located inside this box.

Because the box will move according to the pre-set travel speed v_t and deposition path of the heat source, this allows replicating the creation and deposition of the droplets into the melt pool. The advantage of using this modified version of the double ellipsoid heat source model was recently confirmed by Ling et al. (2021) by avoiding the overheating regions predicted by the standard model.

The use of alternative approaches of computational welding based on the utilization of user-prescribed temperatures T_w of the melt pool (Lindgren et al., 1999) is also used in finite element modelling of WAAM (e.g., Béraud et al., 2022). In case of the latter, an average value of T_w is calculated from the amount of heat supplied to the filler material.

Regardless of the numerical technique used, the proposed value of 50% heat distribution between the base and filler materials must be seen as a first approximation because the distribution can vary from 50% to nearly 20% of the effective efficiency of the heat source in gas metal arc (Fig. 14b), as the wire feed rate v_f increases, considering the energy losses to the surrounding atmosphere and in the welding torch and cabling (Haelsig and Mayr, 2013).

4.3.4. Boundary conditions

Basic modelling conditions in WAAM involve nodal, surface, and symmetrical plane boundary conditions. Nodal boundary conditions consisting of nodes with fixed displacements (or velocities) (Mughal et al., 2006; Ding et al., 2011) or imposed vertical forces (Ahmad et al., 2020) are used to replicate the clamping system applied between the base plate (deformable object) and the backing plate/table (rigid object) where the base plate is attached (Fig. 15a).

Surface boundary conditions are applied to the remaining bottom nodes of the base plate to prevent their movement into the backing plate and, therefore, to avoid penetration of the deformed object into the rigid object (Ding et al., 2011). Removing these constraints at the end of material deposition, (i.e., after removing the physical clamps in the real process), allows calculating the final distortion of the metal part (Fig. 15b).

In the case of heat transfer analysis, surface boundary conditions

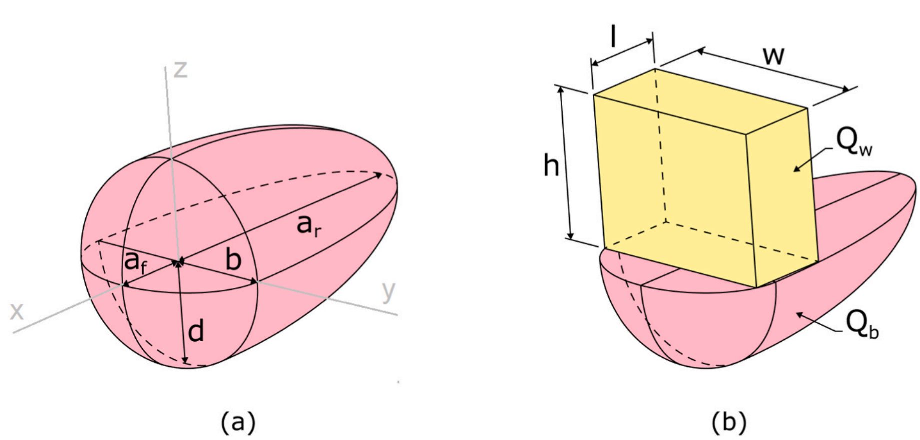

Fig. 14. (a) The double ellipsoid heat source model and (b) its implementation in WAAM.

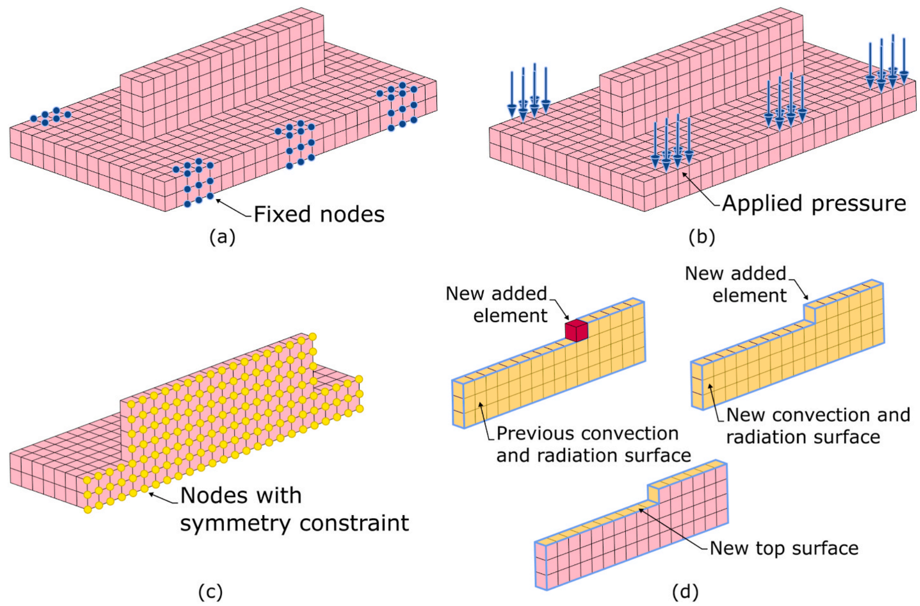

Fig. 15. Boundary conditions in WAAM. (a) nodal, (b) surface and (c) symmetrical plane boundary conditions with (d) a schematic representation of the 'element birth technique'.

consist of assigning free convection and radiation on the top of the base plate and on the walls of the deposited material (Mughal et al., 2006; Montevecchi et al., 2017).

The symmetrical plane boundary conditions are mainly used to reduce the size of the finite element models and the overall CPU requirements. In case of WAAM, they usually consist of halving the base plate and deposited material (deformable objects) and assuming that (i) the normal components of the displacements (or velocities) along the symmetry plane are zero, and (ii) the heat flux across the symmetry plane is also zero (Fig. 15c).

While the first two types of boundary conditions are used, with more or less variants, in most of the finite element WAAM simulations reported in the literature, the third type (symmetry plane) is less common, despite being reported in several papers such as Ding et al. (2011, 2014), Montevecchi et al. (2017) and Saadatmand and Talemi (2020), among others.

Fig. 15d refers to the 'element birth technique' which requires new mesh elements of the deposited material to be progressively activated under the moving heat source. This allows replacing the formation, detachment, and impingement of the molten drops from the arc into the melt pool and mimic the additive nature of WAAM by summing up the new activated elements to the deposited elements already created in the previous time increments.

The reason why this topic was included in this subsection is because the addition of new elements to the previous mesh changes the mechanical and thermal boundary conditions due to the necessity of reconstructing the external surfaces of the deposited metal part and accounting for the heat input of the new added elements.

The element birth technique has roots in computational welding and can be numerically implemented by means of two different approaches, referred to as 'quiet elements' and 'born-dead elements' (Lindgren et al., 1999). The first approach ('quiet elements') contains all the elements of the deposited material defining the successive layers that will be added during the simulation in the initial finite element model. However, these elements are made 'quiet' (passive) by giving them material properties that will not affect the overall thermo-mechanical model (e.g., very low values of the elasticity modulus E and thermal conductivity k), until they become active, and their material properties restored. Examples of the utilization of this technique in WAAM are found in Mughal et al. (2006) and Montevecchi et al. (2016). The latter suggested a methodology for material properties being progressively switched from quiet to active values to avoid convergence problems during the simulations.

The second approach ('born-dead elements') also requires the existence of a mesh containing all the elements of the deposited material defining the successive layers that will be deposited during the simulation. But, in contrast to the previous approach, the elements of the deposited material are excluded in the initial finite element model by not including them in the assembly of the system of equations until they are added (born). Examples of the utilization of this technique in WAAM are found in Xiong et al. (2017), Cambon et al. (2020) and Béraud et al. (2022).

Both approaches have advantages and disadvantages. The first approach requires supplying the 'quiet elements' with very low mechanical and thermal material properties that may give rise to ill-conditioned matrices. Quiet elements also require elimination of possible temperatures, strains and stresses that may have been accumulated up to the instant of activation. However, the approach is easy to implement in existing thermo-mechanical finite element computer programs.

The second approach requires restructuring node and element numbering each time new 'born-dead elements' are activated and allocating new dimensions for the matrices and arrays to include and assemble the new nodes and elements in the thermal and mechanical finite element models. This is the correct approach from a computational point of view but requires the use of finite element programs with this capability.

4.3.5. Analysis type

Thermo-mechanical finite element modelling of WAAM can be coupled or staggered. Although a coupled solution like that used by Tunay et al. (2023) is preferred because of solving thermal and mechanical problems simultaneously, it leads to a single, very large, system of equations that requires significant CPU requirements.

The staggered solution reduces these needs by de-coupling the thermo-mechanical problem into two sub-problems that are solved in sequence within a time increment Δt. This is the reason why most of the numerical simulations of WAAM refer the calculation of the temperature first and then the use of temperature distribution to perform the mechanical analysis of the time increment (e.g., Montevecchi et al., 2016; Saadatmand and Talemi, 2020; Belhadj et al., 2021).

The solution of the thermal problem by finite elements makes use of the following integral form of the governing equation (6), which instead of satisfying the heat transfer equation exactly (that is, pointwise), only fulfils it in an average sense over the entire volume of the domain (metal part),

$$\int_V k\nabla T\nabla(\delta T)dV - \int_{S_q} q_n\delta T dS_q + \int_V \rho c\frac{dT}{dt}\delta T dV - \int_V \dot{Q}\delta T dV = 0 \quad (10)$$

In the above equation the symbol δT denotes an arbitrary variation in the temperature, $q_n = k\nabla T \bullet \boldsymbol{n}$, is the heat flux along the surface S_q (belonging to the closed surface S of the domain), where $\boldsymbol{n}$ is the vector of direction cosines of the normal to the surface S_q, and $\dot{Q}$ is the internal heat generation rate (internal source) containing the power $\dot{Q}_b$ transferred from the heat source model to the base material.

Fig. 16 shows a finite element example of a complete thermal cycle during the deposition of several layers of a vertical wall in an Al–5Mg alloy by WAAM and subsequent cooling (Oyama et al., 2019). The correlation between the numerical and experimental results is good and the same conclusion can be drawn from similar investigations reported in the literature (e.g., Sandeep et al., 2022; Hagen et al., 2023).

The solution of the mechanical problem by finite elements follows a similar strategy to ensure that the equilibrium requirements of the governing equation (7) are written in a weak form that only satisfies the equilibrium conditions in an average sense over the entire domain, (the term 'weak form' results from its weaker continuity requirements compared to those of the governing equation),

$$\int_V \sigma_{ij}\frac{\partial(\delta u_i)}{\partial x_j}dV - \int_{S_t} t_i\delta u_i dS = 0 \quad (11)$$

In the above equation the symbol δu_i denotes an arbitrary variation in the displacement or velocity. This duality results from the finite element implementation being done with displacements or velocities (rate-form). The symbol $t_i = \sigma_{ij}n_j$ denotes the tractions applied on the boundary S_t with the prescribed traction having the unit normal vector n_j.

The above equation (11) together with appropriate constitutive equations for temperature dependent elastic-plastic materials gives rise to the following matrix set of nonlinear equations,

$$\boldsymbol{K}\boldsymbol{u} = \boldsymbol{F} \quad (12)$$

where $\boldsymbol{K}$ is the stiffness matrix and $\boldsymbol{F}$ is the generalized force vector resulting from the applied forces, pressure, and thermal loads.

The thermal loads are caused by temperature changes within a time increment Δt and are included in $\boldsymbol{F}$ as a result of the thermal strain increment $\Delta\varepsilon^t$,

$$\Delta\varepsilon^t = \alpha(T)\Delta T \quad (13)$$

where α is the coefficient of thermal expansion.

The thermal strain increment $\Delta\varepsilon^t$ (13) adds to the elastic strain increment $\Delta\varepsilon^e$, calculated from the elasticity modulus and Poisson ratio, and to the plastic strain increment $\Delta\varepsilon^p$, calculated from the flow curve, to obtain the total increment of strain $\Delta\varepsilon = \Delta\varepsilon^e + \Delta\varepsilon^p + \Delta\varepsilon^t$.

Material dependent properties, thermal strains and flow curve are sources of nonlinearity, but they provide the link between thermal and mechanical solutions of staggered modelling. In connection to this, it is worth noting that some authors (e.g., Denlinger et al., 2015) suggest implementation of a relaxation procedure at element level by resetting the stresses and strains at the previous time increment to zero, when the temperature of an element exceeds a prescribed relaxation temperature T_{relax}. Typical values of the T_{relax} are close to the annealing temperature.

Background to the relaxation procedure is found in the work of Griffith et al. (1998), Qiao et al. (2013) and Song et al. (2014), among others. Griffith et al. (1998) showed that the high temperatures reached in laser deposition of AISI 316 stainless steel cause the material to anneal and to reduce the measured residual stresses. Qiao et al. (2013) performed microhardness measurements to demonstrate that the plastic strain needs to be dynamically adjusted at high temperatures in thermo-elastic-plastic modelling of material annealing. Song et al. (2014) accounted for the plastic strain relaxation at high temperatures in a deposited nickel-based alloy by setting a threshold relaxation temperature beyond which the plastic strain is set to zero.

The displacement (or, velocity) vector $\boldsymbol{u}$ resulting from the solution of the non-linear set of equation (12) at the end of WAAM provides the undesirable dimensional changes (distortions) that are connected to the distribution of residual stresses in equilibrium after unclamping, through the constitutive equation,

$$\sigma_{ij} = C_{ijkl}\left(\varepsilon_{kl} - \varepsilon^p_{kl} - \varepsilon^t_{kl}\right) \quad (14)$$

where C_{ijkl} is the fourth order material stiffness tensor.

Fig. 17 illustrates the link between distortions and residual stresses in WAAM. The latter, according to Hönnige et al. (2018), can range from 60% to almost 100% of the materials' yield stress.

Prediction of residual stresses and distortions in WAAM are provided in several other publications such as, Oyama et al. (2019) and Sun et al. (2021). The correlation between numerical and experimental results is generally good from a geometric perspective but sometimes poor for the residual stress values (Oyama et al., 2019). In most cases, the differences are attributed to problems in boundary conditions and material non-linearity. However, failure to implement relaxation procedures in finite element calculations may also lead to errors in the residual stress values and in-situ distortions of over 500%, as claimed by Denlinger et al. (2015).

4.3.6. Material data

Because temperature in the built metal parts changes significantly

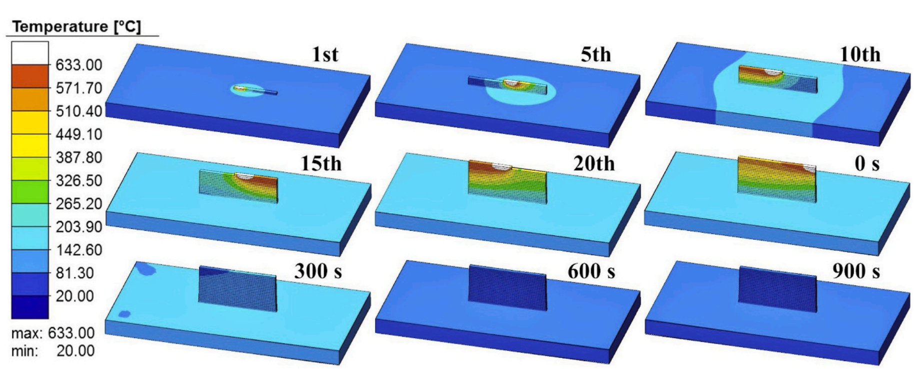

Fig. 16. Evolution of the melt pool size and of the temperature field during the deposition of several layers of a vertical wall by WAAM and subsequent cooling (Oyama et al., 2019).

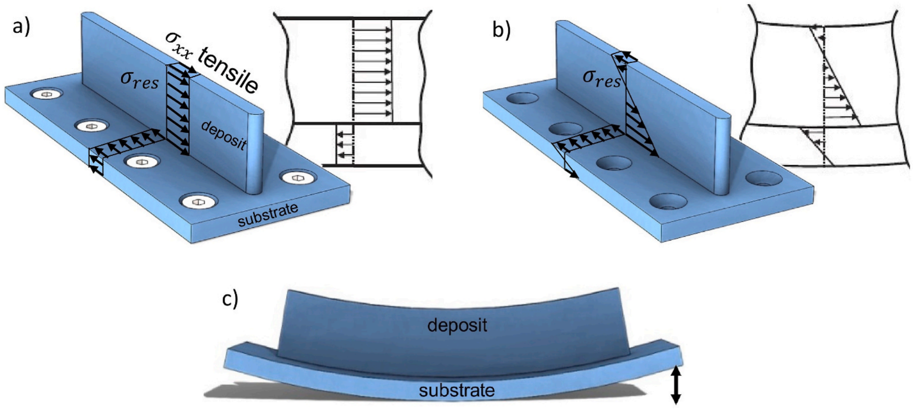

Fig. 17. Schematic representation of the link between residual stresses and distortions in WAAM. (a) Distribution of residual stress when the metal part is clamped, (b) redistributed and balanced distribution of residual stresses upon removal of the clamps and (c) distortion upon removal of the clamps (Hönnige et al., 2018).

from the melt pool to the substrate, it is important to account for the variations of material properties (such as, density, thermal conductivity, specific heat, elasticity modulus, yield stress, Poisson ratio and coefficient of thermal expansion) with temperature, instead of using constant values.

The density ρ of metals generally decreases with increasing temperature. In the case of pure metals, the reduction in density as the temperature rises from 25°C to the melting temperature is approximately 7% before melting, and 12% on complete melting (Firdu and Taskinen, 2010). These small variations explain the reason why many authors do not account for the variation of density with temperature in the finite element modelling of WAAM.

Thermal conductivity k in pure metals stays roughly the same as the temperature rises from 25°C to the melting temperature (Ausloos, 2001). However, in metal alloys the values often increase proportionally to temperature. Some authors do not account for the variation of thermal conductivity with temperature (e.g., Ogino et al., 2018), while others take this variation into consideration (e.g., Xiong et al., 2017 and, Jayanath and Achuthan, 2018; Saadatmand and Talemi, 2020).

Specific heat c presents significant variations with temperature. Although these variations must be properly accounted for in the numerical simulations (e.g., Xiong et al., 2017; Saadatmand and Talemi, 2020), there are publications in which constant values are employed (e.g., Li et al., 2019).

The elasticity modulus E and yield stress σ_Y decrease with the rise in temperature and these variations should also be taken into consideration (e.g., Li et al., 2019; Saadatmand and Talemi, 2020). The Poisson ratio ν of metals increases with the rise in temperature and approaches the limiting value of 0.5 when temperature rises to the melting temperature because the value of the Poisson ratio in the plastic regime is 0.5 (Everett and Miklowitz, 1944).

The coefficient of thermal expansion α increases with temperature. In the case of stainless steel, for example, the increase is below 20% when the temperature rises from 25°C to 700°C.

A practical approach to obtain information on the temperature dependence of material properties is to make use of special purpose commercial software such as CALPHAD and JMatPro. The use of JMatPro to provide material data for the numerical modelling of WAAM is reported in Graf et al. (2018).

4.3.7. Numerical parameters

The non-linear characteristics of the thermo-mechanical finite element modelling of WAAM require calculations to be carried out incrementally, and iteratively within a time increment. The convergence of the iterative procedures is commonly monitored by means of norms built upon displacement vectors $\boldsymbol{u}$ (or velocity vectors in case the equilibrium equation (11) are implemented in the rate form) and temperature T,

$$\frac{\|\boldsymbol{u}_n - \boldsymbol{u}_{n-1}\|}{\|\boldsymbol{u}_n\|} \le \delta_u \qquad \frac{\|T_n - T_{n-1}\|}{\|T_n\|} \le \delta_T \tag{15}$$

where n is the iteration number and δ_u and δ_T are the threshold convergence values typically ranging from 10^{-2} to 10^{-5}, depending on the accuracy requirements for the solution.

Time increment is an important parameter in WAAM due to its direct relation with the numerical procedure to replicate the formation, detachment and impingent of the molten droplets from the arc into the melt pool through the addition of new elements to the previous mesh. Considering the use of a constant power density distribution $\dot{q}_w$ for the filler material, as suggested by Montevecchi et al. (2016), it is possible to rewrite equation (9) in terms of the energy density q_w, as follows,

$$q_w = \frac{\dot{Q}_w}{lwh}\Delta t = \frac{\dot{Q}_w}{v_t wh} \tag{16}$$

The above equation establishes a correspondence between the travel speed v_t of the moving heat source and the time increment $\Delta t = l/v_t$ for the new mesh elements (corresponding to the molten drop) to be inside the assumed box with volume lwh, (refer to sub-section 'Heat source'). This correspondence allows the heat source to transmit the correct amount of energy to the finite element model (Montevecchi et al., 2016).

The use of alternative approaches of computational welding based on the supply of a user-prescribed temperature T_w to the melt pool added elements (Béraud et al., 2022), instead of the energy density q_w, also requires a time increment correspondence $\Delta t = l/v_t$ between the length l of the heat source and the travel speed v_t. This is necessary to ensure compatibility between the prescribed temperature T_w and the energy supplied by the heat source to the melt pool added elements.

However, regardless the type of boundary condition supplied to the new mesh elements (energy or temperature), it is always possible to relate the wire feed rate v_f and the travel speed v_t, as follows (Chiumenti et al., 2010),

$$v_t = \frac{\pi d_f^2}{4wh} v_f \tag{17}$$

where wh is the cross section of the box and d_f the diameter of the wire feedstock.

5. Outlook and conclusions

This state-of-the-art review was focused on the modelling of WAAM. Special emphasis was placed on the finite element method at macro-scale level due to its capability of delivering very efficient computer programs to produce accurate predictions of temperatures, displacements, strains, and stresses.

The widespread utilization of finite elements in WAAM is intended to: (i) increase process know-how, (ii) reduce the amount of trial-and-error setting of the operating parameters, (iii) produce complex metal parts with better quality in shorter time and lower costs and (iv) assist training of technicians and engineers. By focusing on the main ingredients of the pre-processing and numerical solution methods, it was possible to provide readers with the main topics and developments that are currently being worked on by leading researchers in the field while keeping the presentation level in an understandable language.

Most of the published work revealed the use of commercial, instead of home-developed software. This avoids the complexity and time-consuming task of executing the computer implementation of the equations governing the physics of the process but requires knowledge of the fundamentals and good training skills to prevent errors and misjudgement of the computed results.

Most of the applications published in literature refer to linear, multi-layer, depositions and only a few works refer non-linear (typically, cylindrical, e.g., Graf et al., 2018) metal parts. The coming years will certainly see a trend towards material depositions along arbitrary deposition paths to allow modelling the construction of complex metal parts. This trend will likely come with a greater use of tetrahedral meshes due to the challenge of generating good quality hexahedral meshes in complicated geometries.

The move towards complexity and the use of finite element analysis to supply data for training machine learning models also copes with the inevitable growing use of artificial intelligence to determine the optimal operating conditions in WAAM.

Another trend that will emerge in the coming years is the modelling of hybrid additive manufacturing involving WAAM and other manufacturing processes such as metal cutting and metal forming (Pragana et al., 2021b, 2021c). This is a topic for which commercial finite element programs with broader applicability are better prepared than in-house solutions specifically developed for WAAM.

The application of finite element modelling to real industrial metal parts will inevitably raise the issue of accurate temperature dependent material properties and will stimulate the integration of finite element computer programs and material simulation software, to analyse the material solidification behaviour and phase transformations.

Finite element modelling of WAAM at multi-scale level is here to stay and its use is unavoidable to obtain a complete understanding of the physics of the process, even though the required CPU requirements being substantial and unsuitable to simulate the construction of real size metal parts. Still, research in this direction that couples the thermo-mechanical models at macro-scale, with the fluid flow and heat transfer models at meso-scale and the phase field models at micro-scale is ongoing and paving the way to the future (e.g., Bai et al., 2018).

Declaration of competing interest

The authors declare that they have no known competing financial interests or personal relationships that could have appeared to influence the work reported in this paper.

Data availability

No data was used for the research described in the article.

Acknowledgments

The authors would like to acknowledge the support provided by Fundação para a Ciência e a Tecnologia of Portugal and IDMEC under LAETA- UIDB/50022/2020 and PTDC/EME-EME/0949/2020.

References

Ahmad, S.N., Manurung, Y.H.P., Mat, M.F., Minggu, Z., Jaffar, A., Pruller, S., Leitner, M., 2020. FEM simulation procedure for distortion and residual stress analysis of wire-arc additive manufacturing. IOP Conf. Ser. Mater. Sci. Eng. 834, 012083.
Ahn, D.G., 2021. Directed energy deposition (DED) process: state of the art. Int. J. Precis. Eng. Manuf.Green Technol 8, 703–742.
Ausloos, M., 2001. Thermal conductivity. In: Buschow, K.H.J., Cahn, R.W., Flemings, M. C., Ilschner, B., Kramer, E.J., Mahajan, S., Veyssière, P. (Eds.), Encyclopedia of Materials: Science and Technology. Elsevier, pp. 9151–9155.
Bai, X., Colegrove, P., Ding, J., Zhou, X., Diao, C., Bridgeman, P., Hönnige, J.R., Zhang, H., Williams, S., 2018. Numerical analysis of heat transfer and fluid flow in multilayer deposition of PAW-based wire and arc additive manufacturing. Int. J. Heat Mass Tran. 124, 504–516.
Bauer, A., Scharf, R., Hälsig, A., Awiszus, B., 2021. Numerical simulation and calibration of a single seam WAAM process with a commercial and an open source software. J. Appl. Eng.Des.Simul. 1, 25–31.
Baufeld, B., Van der Biest, O., Gault, R., 2010. Additive manufacturing of Ti–6Al–4V components by shaped metal deposition: microstructure and mechanical properties. Mater. Des. 31, 106–111.
Belhadj, M., Werda, S., Belhadj, A., Kromer, R., Darnis, P., 2021. Thermal analysis of wire arc additive manufacturing process. In: 24th International Conference on Material Forming - ESAFORM 2021, p. 4095. Liège, Belgium.
Béraud, N., Chergui, A., Limousin, M., Villeneuve, F., Vignat, F., 2022. An indicator of porosity through simulation of melt pool volume in aluminum wire arc additive manufacturing. Mechanics & Industry 23, 1.
Cadiou, S., Courtois, M., Carin, M., Berckmans, W., Le Masson, P., 2020. Heat transfer, fluid flow and electromagnetic model of droplets generation and melt pool behaviour for wire arc additive manufacturing. Int. J. Heat Mass Tran. 148, 119102.
Cambon, C., Rouquette, S., Bendaoud, I., Bordreuil, C., Wimpory, R., Soulie, F., 2020. Thermo-mechanical simulation of overlaid layers made with wire + arc additive manufacturing and GMAW-cold metal transfer. Weld. World 64, 1427–1435.
Chiumenti, M., Cervera, M., Salmi, A., Saracibar, C.A., Dialami, N., Matsui, K., 2010. Finite element modeling of multi-pass welding and shaped metal deposition processes. Comput. Methods Appl. Mech. Eng. 199 (239), 2343.
Chowdhury, S., 2013. Artificial Neural Network Based Geometric Compensation for Thermal Deformation in Additive Manufacturing Processes. MSc Thesis. Manipal Institute of Technology, Karnataka, India.
Chu, J.B., 2014. Investigating the Feasibility and Impact of Integrating Wire-Arc Additive Manufacturing in Aerospace Tooling Applications. MSc Thesis, University of Michigan, Michigan.
Cunningham, C.R., Flynn, J.M., Shokrani, A., Dhokia, V., Newman, S.T., 2018. Invited review article: strategies and processes for high quality wire arc additive manufacturing. Addit. Manuf. 22, 672–686.
DebRoy, T., Wei, H.L., Zuback, J.S., Mukherjee, T., Elmer, J.W., Milewski, J.O., Beese, A. M., Wilson-Heid, A., De, A., Zhang, W., 2018. Additive manufacturing of metallic components–process, structure and properties. Prog. Mater. Sci. 92.
Deckard, C.R., 1989. Method and apparatus for producing parts by selective sintering. U. S. Patent No. 4, 863, 538. Washington, DC: U.S. Patent and Trademark Office.
Denlinger, E.R., Irwin, J., Michaleris, P., 2014. Thermomechanical modeling of additive manufacturing large parts. J. Manuf. Sci. Eng. 136, 061007.
Denlinger, E.R., Heigel, J.C., Michaleris, P., 2015. Residual stress and distortion modeling of electron beam direct manufacturing Ti-6Al-4V. J. Eng. Manufact. 229, 1803–1813.
Derekar, K.S., 2018. A review of wire arc additive manufacturing and advances in wire arc additive manufacturing of aluminium. Mater. Sci. Technol. 34, 895–916.
Dias, M., Pragana, J.P., Ferreira, B., Ribeiro, I., Silva, C.M., 2022. Economic and environmental potential of wire-arc additive manufacturing. Sustainability 14, 5197.
Dickens, P.M., Pridham, M.S., Cobb, R.C., Gibson, I., Dixon, G., 1992. Rapid Prototyping Using 3-D Welding. 1992 International Solid Freeform Fabrication Symposium.
Ding, J., Colegrove, P., Mehnen, J., Ganguly, S., Sequeira Almeida, P.M., Wang, F., Williams, S., 2011. Thermo-mechanical analysis of wire and arc additive layer manufacturing process on large multi-layer parts. Comput. Mater. Sci. 50, 3315–3322.
Ding, J., Colegrove, P., Mehnen, J., Williams, S., Wang, F., Sequeira Almeida, P., 2014. A computationally efficient finite element model of wire and arc additive manufacture. Int. J. Adv. Manuf. Technol. 70, 227–236.
Ding, D., Pan, Z., Cuiuri, D., Li, H., 2015. Wire-feed additive manufacturing of metal components: technologies, developments and future interests. Int. J. Adv. Manuf. Technol. 81, 465–481.
Ding, D., Pan, Z., Cuiuri, D., Li, H., van Duin, S., Larkin, N., 2016. Bead modelling and implementation of adaptive MAT path in wire and arc additive manufacturing. Robot. Comput. Integrated Manuf. 39, 32–42.
Dinovitzer, M., Chen, X., Laliberte, J., Huang, X., Frei, H., 2019. Effect of wire and arc additive manufacturing (WAAM) process parameters on bead geometry and microstructure. Addit. Manuf. 26, 138–146.
Everett, F.L., Miklowitz, M.J., 1944. Poisson's ratio at high temperatures. J. Appl. Phys. 15, 592–597.
Fan, H.G., Kovacevic, R., 1999. Droplet formation, detachment, and impingement on the molten pool in gas metal arc welding. Metall. Mater. Trans. B 30, 791–801.
Feng, Y., Zhan, B., He, J., Wang, K., 2018. The double-wire feed and plasma arc additive manufacturing process for deposition in Cr-Ni stainless steel. J. Mater. Process. Technol. 259, 206–215.
Firdu, F.T., Taskinen, P., 2010. Densities of Molten and Solid Alloys of (fe, Cu, Ni, Co) - S at Elevated Temperatures - Literature Review and Analysis. Aalto University

Publications in Materials Science and Engineering, Aalto University School of Science and Technology, Finland.
Gibson, I., Rosen, D., Stucker, B., 2015. Directed energy deposition processes. In: Additive Manufacturing Technologies – 3D Printing, Rapid Prototyping, and Direct Digital Manufacturing. Springer, Berlin, pp. 245–268.
Goldak, J., Akhlaghi, M., 2005. Computational Welding Mechanics. Springer, New York.
Goldak, J., Chakravarti, A., Bibby, M.A., 1984. A new finite element model for welding heat sources. Metall. Trans. A B 15B, 299–305.
Graf, M., Hälsig, A., Höfer, K., Awiszus, B., Mayr, P., 2018. Thermo-mechanical modelling of wire-arc additive manufacturing (WAAM) of semi-finished products. Metals 8, 1009.
Griffith, M., Schlienger, M., Harwell, L., 1998. Thermal Behavior in the LENS Process. In: Proceedings of the Solid Freeform Fabrication Symposium. University of Texas, Austin, USA, pp. 89–97.
Hackenhaar, W., Mazzaferro, J.A.E., Montevecchi, F., Campatelli, G., 2020. An experimental-numerical study of active cooling in wire arc additive manufacturing. J. Manuf. Process. 52, 58–65.
Haelsig, A., Mayr, P., 2013. Energy balance study of gas-shielded arc welding processes. Weld. World 57, 727–734.
Hagen, L., Yu, Z., Clarke, A., Clarke, K., Tate, S., Petrella, A., Klemm-Toole, J., 2023. High deposition rate wire-arc directed energy deposition of 316L and 316LSi: process exploration and modelling. Mater. Sci. Eng., A, 145044.
Hönnige, J.R., Colegrove, P.A., Ahmad, B., Fitzpatrick, M.E., Ganguly, S., Lee, T.L., Williams, S.W., 2018. Residual stress and texture control in Ti-6Al-4V wire + arc additively manufactured intersections by stress relief and rolling. Mater. Des. 150, 193–205.
Hu, J., Tsai, H.L., 2007b. Heat and mass transfer in gas metal arc welding. Part I: the arc. Int. J. Heat Mass Tran. 50, 833–846.
Hu, J., Tsai, H.L., 2007a. Heat and mass transfer in gas metal arc welding. Part II: the metal. Int. J. Heat Mass Tran. 50, 808–820.
Israr, R., Buhl, J., Bambach, M., 2021. A study on power-controlled wire-arc additive manufacturing using a data-driven surrogate model. Int. J. Adv. Manuf. Technol. 117, 2133–2147.
ISO/ASTM 52900, 2015. Additive Manufacturing—General Principles—Terminology.
Jayanath, S., Achuthan, A., 2018. A computationally efficient finite element framework to simulate additive manufacturing processes. J. Manuf. Sci. Eng. 140, 041009.
Jia, C., Liu, W., Chen, M., Guo, M., Wu, S., Wu, C., 2020. Investigation on arc plasma, droplet, and molten pool behaviours in compulsively constricted WAAM. Addit. Manuf. 34, 101235.
Jin, W., Zhang, C., Jin, S., Tian, Y., Wellmann, D., Liu, W., 2020. Wire arc additive manufacturing of stainless steels: a review. Appl. Sci. 10, 1563.
Karlsson, R.I., Josefson, B.L., 1990. Three-dimensional finite element analysis of temperatures and stresses in a single-pass butt welded pipe. J. Pressure Vessel Technol. 112, 77–84.
Krutz, W.G., Segerlind, J.L., 1976. Finite Element Analysis of Welded Structures. Welding Research Supplement, pp. 211–216.
Lavery, N.P., Brown, S.G.R., Sienz, J., Cherry, J., Belblidia, F., 2014. A review of computational modelling of additive layer manufacturing – multi-scale and multi-physics. In: Proceedings of the International Conference on Sustainable Design and Manufacturing Cardiff, pp. 668–690. UK.
Lee, J.Y., An, J., Chua, C.K., 2017. Fundamentals and applications of 3D printing for novel materials. Appl. Mater. Today 7, 120–133.
Li, Y., Sun, Y., Han, Q., Zhang, Q., Horváth, I., 2018. Enhanced beads overlapping model for wire and arc additive manufacturing of multi-layer multi-bead metallic parts. J. Mater. Process. Technol. 252, 838–848.
Li, R., Xiong, J., Lei, Y., 2019. Investigation on thermal stress evolution induced by wire and arc additive manufacturing for circular thin-walled parts. J. Manuf. Process. 40, 59–67.
Li, Y., Su, C., Zhu, J., 2022. Comprehensive review of wire arc additive manufacturing: hardware system, physical process, monitoring, property characterization, application and future prospects. Res.Eng 13, 100330.
Lindgren, L.E., Runnemalm, H., Nässtöm, M.O., 1999. Simulation of multipass welding of a thick plate. Int. J. Numer. Methods Eng. 44, 1301–1316.
Ling, Y., Ni, J., Abdel Wahab, M., Antonissen, J., Vande Voorde, J., 2021. A heat transfer finite element model for wire-arc-additive-manufacturing process. In: Proceedings of the 8th International Conference on Fracture, Fatigue and Wear. Springer, pp. 201–215.
Liu, Cm, Gao, Hb, Li, Ly, Wang, Jd, Guo, Ch, Jiang, Fc, 2021. A review on metal additive manufacturing: modeling and application of numerical simulation for heat and mass transfer and microstructure evolution. China Foundry 18, 317–334.
Liu, J., Xu, Y., Ge, Y., Hou, Z., Chen, S., 2020. Wire and arc additive manufacturing of metal components: a review of recent research developments. Int. J. Adv. Manuf. Technol. 111, 149–198.
Martina, F., Mehnen, J., Williams, S.W., Colegrove, P., Wang, F., 2012. Investigation of the benefits of plasma deposition for the additive layer manufacture of Ti–6Al–4V. J. Mater. Process. Technol. 212 (6), 1377–1386.
Messler, R.W., 2004. Principles of Welding: Processes, Physics, Chemistry and Metallurgy. Wiley-VCH Verlag, Weinheim.
Mohebbi, M.S., Kühl, M., Ploshikhin, V., 2020. A thermo-capillary-gravity model for geometrical analysis of single-bead wire and arc additive manufacturing (WAAM). Int. J. Adv. Manuf. Technol. 109, 877–891.
Mokrov, O., Simon, M., Schiebahn, A., Reisgen, U., 2019. A fine modification of the double ellipsoid heat source. Mathematical Modelling of Weld Phenomena 12. Verlag der Technischen Universität Graz, Austria.
Montevecchi, F., Venturini, G., Scippa, A., Campatelli, G., 2016. Finite element modelling of Wire-Arc-Additive-Manufacturing process. Procedia CIRP 55, 109–114.
Montevecchi, F., Venturini, G., Grossi, N., Scippa, A., Campatelli, G., 2017. Finite element mesh coarsening for effective distortion prediction in wire arc additive manufacturing. Addit. Manuf. 18, 145–155.
Mughal, M.P., Fawad, H., Mufti, R.A., 2006. Three-dimensional finite-element modelling of deformation in weld-based rapid prototyping. J. Mech. Eng. Sci. 220, 875–885.
Nasiri, M.B., Enzinger, N., 2019. An analytical solution for temperature distribution in fillet arc welding based on an adaptive function. Weld. World 63, 409–419.
Nielsen, C.V., Martins, P.A.F., 2021. Finite element flow formulation. In: Metal Forming: Formability, Simulation and Tool Design. Academic Press, Elsevier, New York, pp. 181–247.
Nijhuis, B., Geijselaers, H.J.M., van den Boogaard, A.H., 2021. Efficient thermal simulation of large-scale metal additive manufacturing using hot element addition. Comput. Struct. 245, 106463.
Ogino, Y., Asai, S., Hirata, Y., 2018. Numerical simulation of WAAM process by a GMAW weld pool model. Weld. World 62, 393–401.
Oyama, K., Diplas, S., M'hamdi, M., Gunnæs, A.E., Azar, A.S., 2019. Heat source management in wire-arc additive manufacturing process for Al-Mg and Al-Si alloys. Addit. Manuf. 26, 180–192.
Pattanayak, S., Sahoo, S.K., 2021. Gas metal arc welding based additive manufacturing—a review. CIRP.J. Manuf. Sci. Technol. 33, 398–442.
Pinkerton, A.J., Li, L., 2004. Modelling the geometry of a moving laser melt pool and deposition track via energy and mass balances. J. Phys. Appl. Phys. 37, 1885–1895.
Pragana, J.P., Bragança, I.M., Reis, L., Silva, C.M., Martins, P.A., 2021a. Formability of wire-arc deposited AISI 316L sheets for hybrid additive manufacturing applications. J. Mater.: Design and Applications 235, 2839–2850.
Pragana, J.P., Bragança, I.M., Silva, C.M., Martins, P.A., 2021b. Integration of tube end forming in wire arc additive manufacturing: an experimental and numerical investigation. Int. J. Adv. Des. Manuf. Technol. 117, 2715–2726.
Pragana, J.P.M., Sampaio, R.F.V., Bragança, I.M.F., Silva, C.M.A., Martins, P.A.F., 2021c. Hybrid metal additive manufacturing: a state–of–the-art review. Adv. Ind.Manuf. Eng. 2, 100032.
Pragana, J.P.M., Rosa, L.G., Bragança, I.M.F., Silva, C.M.A., Tekkaya, A.E., Martins, P.A. F., 2022. Expansion of additive-manufactured tubes: deformation and metallurgical analysis. Steel Res. Int. 93, 2100362.
Provatas, N., Elder, K., 2010. Phase-field methods in materials science and engineering. Wiley-VCH Verlag, Weinheim, Germany.
Qiao, D., Feng, Z., Zhang, W., Wang, Y., Crooker, P.J., 2013. Modeling of weld residual plastic strain and stress in dissimilar metal butt weld in nuclear reactors. In: Proceedings of the ASME 2013 Pressure Vessels and Piping Conference. Paris, France PVP2013-98081.
Raut, L.P., Taiwade, R.V., 2021. Wire arc additive manufacturing: a comprehensive review and research directions. J. Mater. Eng. Perform. 30, 4768–4791.
Ríos, S., Colegrove, P.A., Martina, F., Williams, S.W., 2018. Analytical process model for wire+arc additive manufacturing. Addit. Manuf. 21, 651–657.
Rodrigues, T.A., Duarte, V., Miranda, R.M., Santos, T.G., Oliveira, J.P., 2019. Current status and perspectives on wire and arc additive manufacturing (WAAM). Materials 12, 1121.
Rosenthal, D., 1946. The theory of moving sources of heat and its application to metal treatments. J. Fluids Eng., Trans ASME. 68, 849–865.
Saadatmand, M., Talemi, R., 2020. Study on the thermal cycle of wire arc additive manufactured (WAAM) carbon steel wall using numerical simulation. Frat. Ed. Integrità Strutt. 52, 98–104.
Sachs, E.M., Haggerty, J.S., Cima, M.J., Williams, P.A., 1993. U.S. Patent No. 5,204,055. U.S. Patent and Trademark Office, Washington, DC.
Sandeep, K.J., Teja, P.J., Choudhary, A.K., Jain, R., 2022. Development of correlation between temperature, liquid life span, molten pool, and porosity during Wire Arc Additive Manufacturing: a finite element approach. CIRP.J. Manuf. Sci. Technol. 38, 274–287.
Savyasachi, N., Richard, S., James, J.T., Thomas, D., Ashok, A., 2020. A review on wire and arc additive manufacturing (WAAM). Int.Res.J.Eng.Technol. 7, 4981–4989.
Singh, S.R., Khanna, P., 2021. Wire arc additive manufacturing (WAAM): a new process to shape engineering materials. Mater. Today: Proc. 44, 118–128.
Song, X., Xie, M., Hofmann, F., Illston, T., Connolley, T., Reinhard, C., Atwood, R.C., Connor, L., Drakopoulos, M., Frampton, L., Korsunsky, A.M., 2014. Residual stresses and microstructure in powder bed direct laser deposition (PB DLD) samples. Int. J. Material Form. 10, 1–10.
Srivastava, S., Garg, R.K., Sachdeva, A., Sharma, V.S., 2022. A multi-tier layer-wise thermal management study for long-scale wire-arc additive manufacturing. J. Mater. Process. Technol. 306, 117651.
Sun, J., Hensel, J., Köhler, M., Dilger, K., 2021. Residual stress in wire and arc additively manufactured aluminum components. J. Manuf. Process. 65, 97–111.
Tangestani, R., Farrahi, G.H., Shishegar, M., Aghchehkandi, B.P., Ganguly, S., Mehmanparast, A., 2020. Effects of vertical and pinch rolling on residual stress distributions in wire and arc additively manufactured components. J. Mater. Eng. Perform. 29, 2073–2084.
Tekriwal, P., Mazumder, J., 1988. Finite element analysis of three-dimensional transient heat transfer in GMA welding. Weld J. 67, 150s–156s.
Tomar, B., Shiva, B., Nath, T., 2022. A review on wire arc additive manufacturing: processing parameters, defects, quality improvement and recent advances. Mater. Today Commun. 31, 103739.
Treutler, K., Wesling, V., 2021. The current state of research of wire arc additive manufacturing (WAAM): a review. Appl. Sci. 11, 8619.
Tunay, M., Baykasoğlu, C., Akyildiz, O., To, A.C., 2023. A fully coupled thermal–microstructural–mechanical finite element process model for directed energy deposition additive manufacturing of Ti–6Al–4V. Sci. Technol. Weld. Join. 28, 118–127.

Vartanian, K., Brewer, L., Manley, K., Cobbs, T., 2018. Powder bed fusion vs. Directed energy deposition benchmark study: mid-size part with simple geometry. Optomec Corporation, USA, pp. 1–4.
Wang, G., Huang, P.G., Zhang, Y.M., 2003. Numerical analysis of metal transfer in gas metal arc welding. Metall. Mater. Trans. B 34, 345–353.
Watt, D.F., Coon, L.A., Bibby, M., Goldak, J.A., Henwood, C., 1988. An algorithm for modelling microstructural development in weld heat-affected zones (Part a) reaction kinetics. Acta Metall. 36, 3029–3035.
Wells, A., 1952. Heat flow in welding. Weld J. 31, 263–267.
Williams, S.W., Martina, F., Addison, A.C., Ding, J., Pardal, G., Colegrove, P., 2016. Wire + arc additive manufacturing. Mater. Sci. Technol. 32 (7), 641–647.
Wu, B., Pan, Z., Ding, D., Cuiuri, D., Li, H., Xu, J., Norrish, J., 2018. A review of the wire arc additive manufacturing of metals: properties, defects and quality improvement. J. Manuf. Process. 35, 127–139.
Xiong, J., Lei, T., Li, R., 2017. Finite element analysis and experimental validation of thermal behavior for thin-walled parts in GMAW-based additive manufacturing with various substrate preheating temperatures. Appl. Therm. Eng. 126, 43–52.
Yang, H., Wu, C., Li, H.W., Fan, X.G., 2011. Review on cellular automata simulations of microstructure evolution during metal forming process: grain coarsening, recrystallization and phase transformation. Sci. China Technol. Sci. 54, 2107 – 2118.
Zavarise, G., Wriggers, P., 1998. A segment-to-segment contact strategy. Math. Comput. Model. 28, 497–515.
Zhang, H., Xu, J., Wang, G., 2003. Fundamental study on plasma deposition manufacturing. Surf. Coating. Technol. 171 (1–3), 112–118.